Supporting Information

An Overlooked yet Ubiquitous Fluoride Congenitor: Binding Bifluoride in Triazolophanes using Computer-Aided Design

Raghunath O. Ramabhadran,[⊥] *Yun Liu,*[⊥] *Yuran Hua, Moira Ciardi,*
Amar H. Flood, Krishnan Raghavachari**
Department of Chemistry, Indiana University, 800 East Kirkwood Avenue, Bloomington, IN 47405, USA

Emails of corresponding authors: kraghava@indiana.edu, aflood@indiana.edu

S.1 GENERAL METHODS
S.2 SYNTHESIS OF MACROCYCLE 2
S.3 ^{1}H NMR TITRATIONS OF MACROCYCLE 1
S.4 CHARACTERIZATIONS OF FLUORINE SPECIES
S.5 ION PAIR DETERMINATION OF TETRABUTYLAMMONIUM BIFLUORIDE
S.6 VARIABLE CONCENTRATION ^{1}H NMR STUDIES OF TBA•1_2•HF_2
S.7 COMPUTATIONAL RESULT OF 3•HF_2^-
S.8 ANALYSIS OF THE BINDING MODES OF 1•HF_2^- IN SOLUTION
S.9 UV-VIS TITRATIONS OF MACROCYCLE 1 WITH BIFLUORIDE AND CHLORIDE
S.10 SPECIATION CURVES OF MACROCYCLE 1
S.11 COMPUTATIONAL RESULTS OF 5•HF_2^-, 6•HF_2^-, 4•HF_2^- & 4•Cl^-
S.12 ^{1}H NMR TITRATIONS OF MACROCYCLE 2
S.13 2D NMR CHRACTARIZARION OF 2•HF_2^- & 2•Cl^-
S.14 UV-VIS TITRATIONS OF MACROCYCLE 2 WITH BIFLUORIDE AND CHLORIDE
S.15 VARIABLE CONCENTRATION STUDIES OF MACROCYCLE 2
S.16 SPECIATION CURVES OF MACROCYCLE 2
S.17 NMR SPECTRA OF SYNTHESIZED COMPOUNDS
S.18 DISPERSION EFFECTS AND RELATIVE SOLVATION ENERGIES

S.1 GENERAL METHODS

All reagents were obtained from commercial suppliers and used as received unless otherwise noted. Triazolophane **1**,[S1] protected bisalkyne **7**,[S2] diazide **10**[S1] and **12**[S3] were prepared according to literature procedures. Column chromatography was performed on silica gel (160–200 mesh) and neutral alumina (32–63 μm). Thin-layer chromatography (TLC) was performed on precoated silica gel plates (0.25 mm thick, 60F254, Merck, Germany) and observed under UV light. Nuclear magnetic resonance (NMR) spectra were recorded on Varian Inova (500 MHz), Varian Inova (400 MHz), and Varian VXR (400 MHz) spectrometers at room temperature (298 K). Chemical shifts were referenced to the residual solvent peaks. Electronic absorption spectra were measured on a Varian Cary 5000 UV-Vis-NIR spectrophotometer. High resolution electrospray ionization (ESI) mass spectrometry was performed on a Thermo Electron Corporation MAT 95XP-Trap mass spectrometer. Titration data was analyzed in Sivvu™.[S4] Corresponding speciation curves were generated using Hyss.

All computations have been carried out using the Gaussian suite of programs.[S5] All the geometries have been optimized using the M06-2X functional.[S6] Vibrational frequencies, zero point corrections and thermal corrections have been evaluated using the 6-31+G(d,p) basis set. Unless stated, all the structures are confirmed to be minimum energy structures with no imaginary frequencies. The basis set superposition errors (BSSE) on the computed interaction energies were evaluated using the standard counterpoise method.[S7] Single point energy calculations were carried out subsequently using the significantly larger 6-311++G(3df,2p) basis sets to obtain the anion binding energies. Implicit solvent computations were performed using the SMD model for the optimized geometries in the gas-phase at the M06-2X/6-311++G(3df,2p) level of theory. Finally, Grimme's dispersion corrections to the M06-2X functional were also added to the computed energies and the effects were found to be minimal.

S.2 SYNTHESIS OF MACROCYCLE 2

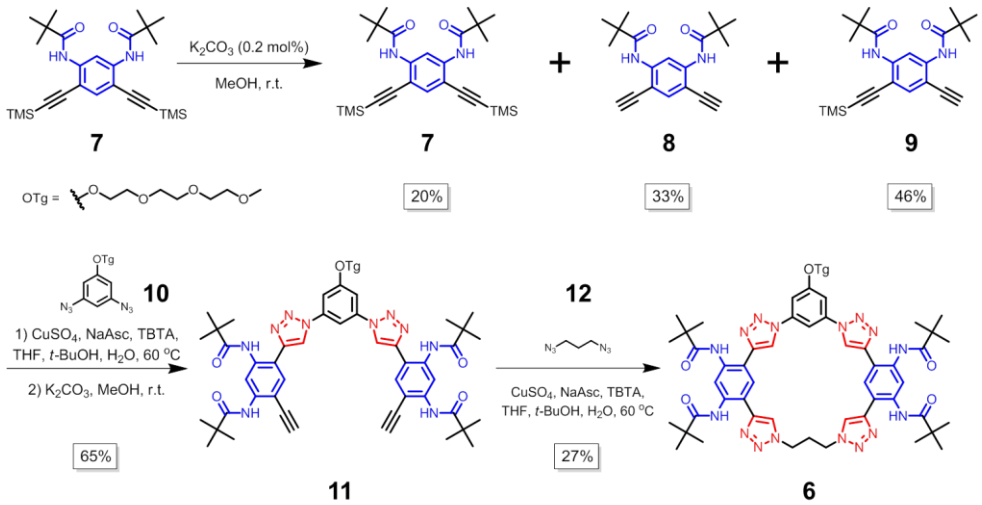

Scheme S1. Syntheses of macrocycle **2** (NaAsc: sodium ascorbate; TMS: trimethylsily; TBTA: tris[(1-benzyl-1H-1,2,3-triazol-4-yl)methyl]amine).

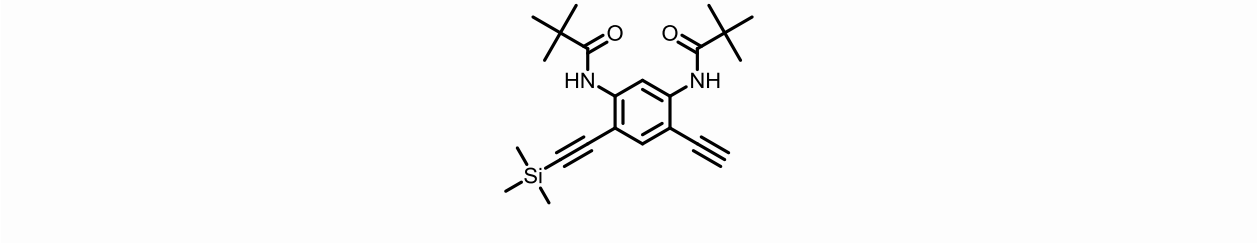

***N,N'*-(4-Ethynyl-6-((trimethylsilyl)ethynyl)-1,3-phenylene)bis(2,2-dimethylpropanamide)** (**9**): Protected bisalkyne (**7**, 4.31g, 9.2 mmol) was dissolved in MeOH (100 mL). The solution was degassed with argon for 10 min, after which K_2CO_3 (2.5 mg, 18.4 mmol) was added and stirred vigorously at room temperature for 20 min. The suspension was poured into hexanes (100 mL). Ethyl acetate (100 mL) and saturated NH_4Cl aqueous solutions (100 mL) were then added. The organic layer was collected, washed with water (2 × 100 mL), dried over Na_2SO_4, filtered through glass wool and concentrated *in vacuo*. The yellowish solid was purified by column chromatography (SiO_2, hexanes to 4:1 hexanes:acetone) to afford **9** (1.69 g, 4.3 mmol) as a pale yellow solid. Yield: 46%. Protected (**7**, 0.87g, 1.9 mmol) and deprotected bisalkynes (**8**, 1.0 g, 3.1 mmol) were recovered during the chromatography. Yield: 20% and 33%. ^{1}H NMR ($CDCl_3$, 400 MHz), δ = 9.60 (s, 1H), 8.34 (s, 1H), 8.26 (s, 1H), 7.46 (s, 1H), 3.47 (s, 1H), 1.28 (s, 9H), 1.27 (s, 9H), 0.23 (s, 9H). ^{13}C NMR ($CDCl_3$, 100 MHz), δ = 175.98, 175.91, 140.99, 140.97, 134.59, 108.99, 106.24, 104.98, 101.47, 99.16, 83.78, 78.37, 40.12, 27.39, 27.34, –0.23. HR-ESI-MS: $C_{23}H_{32}N_2O_2SiNa$ $(M+Na)^+$, Calculated: 419.2131; Found: 419.2138.

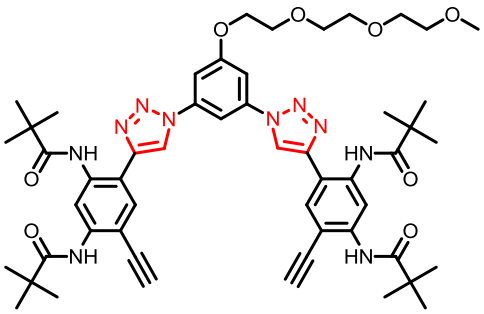

Pentad 11: Monodeprotected bisalkyne **9** (196.7 mg, 0.49 mmol) and diazide **10** (80 mg, 0.25 mmol) were dissolved in a solvent mixture of *t*-BuOH:THF:H_2O (3:3:1, 25 mL). The solution was degassed with argon at 60 ^oC for 30 min, after which TBTA (26.2 mg, 0.05 mmol), NaAsc (29.5 mg, 0.15 mmol) and $CuSO_4$•$5H_2O$ (12.4 mg, 0.05 mmol) were added and stirred at 60 ^oC for 2 h. The volatiles were then removed *in vacuo* and the residuals were extracted with dichloromethane (100 mL). The organic layer was washed with EDTA aqueous solution (50 mL) and water (50 mL), dried over Na_2SO_4, filtered and concentrated *in vacuo*. The resulting pale yellow solid was dissolved in tetrahydrofuran (THF, 20 mL) and a saturated K_2CO_3 solution in MeOH (1 mL) was added. The solution was stirred at room temperature for 30 min, after which the solvent was removed *in vacuo*. The crude product was extracted in dichloromethane (50 mL) and water (50 mL). The organic layer was separated, washed with water (50 mL), dried over Na_2SO_4, filtered and concentrated *in vacuo*. The resulting pale yellow solid was purified by column chromatography (SiO_2, hexanes:acetone: 3:1 to 1:1) to afford **11** (156.7 mg, 0.16 mmol) as a pale yellow solid. Yield: 65%. ^{1}H NMR ($CDCl_3$, 400 MHz), δ = 11.43 (s, 2H), 9.77 (s, 2H),

8.73 (s, 2H), 8.20 (s, 1H), 8.15 (s, 2H), 7.69 (s, 2H), 7.53 (s, 2H), 4.40–4.30 (m, 4H), 3.99–3.85 (m, 4H), 3.77 (dd, J = 5.4, 3.4 Hz, 2H), 3.70 (dd, J = 5.6, 3.4 Hz, 2H), 3.66 (dd, J = 5.5, 3.7 Hz, 2H), 3.55 (dd, J = 5.6, 3.6 Hz, 2H), 3.48 (s, 2H), 3.35 (s, 3H), 1.39 (s, 18H), 1.19 (s, 18H). ^{13}C NMR ($CDCl_3$, 100 MHz), δ = 178.01, 176.14, 160.62, 146.92, 140.04, 138.28, 130.16, 119.33, 112.41, 111.11, 106.80, 105.33, 104.28, 84.03, 78.97, 71.84, 70.85, 70.58, 70.49, 69.39, 68.60, 58.91, 40.48, 40.10, 27.76, 27.41. HR-ESI-MS: $C_{53}H_{66}N_{10}O_8Na$ $(M+Na)^+$, Calculated: 993.4963; Found: 993.4953.

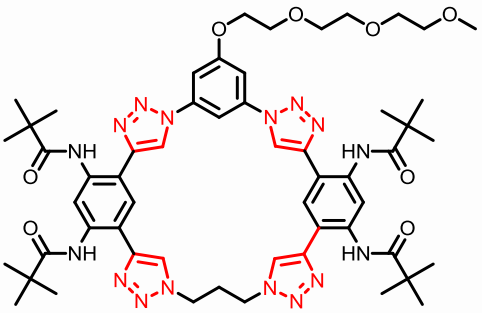

Macrocycle 2: To a degassed solvent mixture of *t*-BuOH:THF:H_2O (3:1:1, 50 mL) was added reagents TBTA (10.9 mg, 0.021 mmol), NaAsc (12.2 mg, 0.062 mmol) and $CuSO_4$•$5H_2O$ (7.7 mg, 0.031 mmol). The pentad **11** (101.7 mg, 0.10 mmol) and 1,3-diazidopropane **12** (13.2 mg, 0.10 mmol) were dissolved in the same solvent mixture of *t*-BuOH:THF:H_2O (3:1:1, 50 mL) and degassed with argon for 30 min. This solution of **11** and **12** was taken up by a 60 mL syringe and pumped into the previously degassed solution of reagents over 10 h at 60 ^{o}C under argon. The volatiles were removed *in vacuo*. The crude product was extracted in dichloromethane (100 mL) and water (50 mL). The organic layer was separated, washed with water (50 mL), dried over Na_2SO_4, filtered and concentrated *in vacuo*. The resulting pale yellow solid was purified by preparative thin layer chromatography (1 mm SiO_2, 3% MeOH in dichloromethane × 2) to afford **2** (30 mg, 0.027 mmol) as a white solid. Yield: 27%. ^{1}H NMR ($CDCl_3$, 500 MHz, with 10 equivalents. of tetra-*n*-butylammonium chloride), δ = 11.73 (s, 2H), 11.52 (s, 2H), 10.67 (s, 2H), 10.14 (s, 2H), 10.04 (s, 2H), 8.82 (s, 2H), 8.76 (s, 1H), 7.88 (s, 2H), 4.57–4.52 (m, 4H), 4.37–4.32 (m, 2H), 3.98–3.92 (m, 2H), 3.83–3.75 (m, 2H), 3.76–3.69 (m, 3H), 3.69–3.65 (m, 2H), 3.60–3.55 (m, 2H), 3.04–2.92 (m, 2H), 1.43 (s, 9H, buried under □-TBA^+), 1.25 (s, 9H). ^{13}C NMR ($CDCl_3$, 125 MHz), δ = 178.13, 178.04, 159.49, 145.99, 144.51, 136.29, 136.15, 127.70, 124.53, 118.71, 117.23, 113.85, 112.20, 111.22, 103.72, 100.81, 70.82, 70.46, 69.98, 69.85, 68.64, 67.79, 59.12, 45.70, 40.51, 29.63, 27.70, 27.64. HR-ESI-MS: $C_{56}H_{72}N_{16}OCl$ $(M+Cl)^-$, Calculated: 1131.5408; Found: 1131.5406.

S.3 ^{1}H NMR TITRATIONS OF MACROCYCLE 1

The titration of macrocycle **1** with tetra-*n*-butylammonium bifluoride ($TBAHF_2$) was monitored by ^{1}H NMR spectroscopy at room temperature (298 K). 400 μL of 2 mM (or 0.5 mM) macrocycle solutions were prepared in screw-cap NMR tubes equipped with PTFE/silicone septa. Aliquots of 80 mM (or 20 mM) $TBAHF_2$ solutions in screw-cap vials equipped with PTFE/silicone septa were added using 10 μL and 100 μL gas-tight micro-syringes.

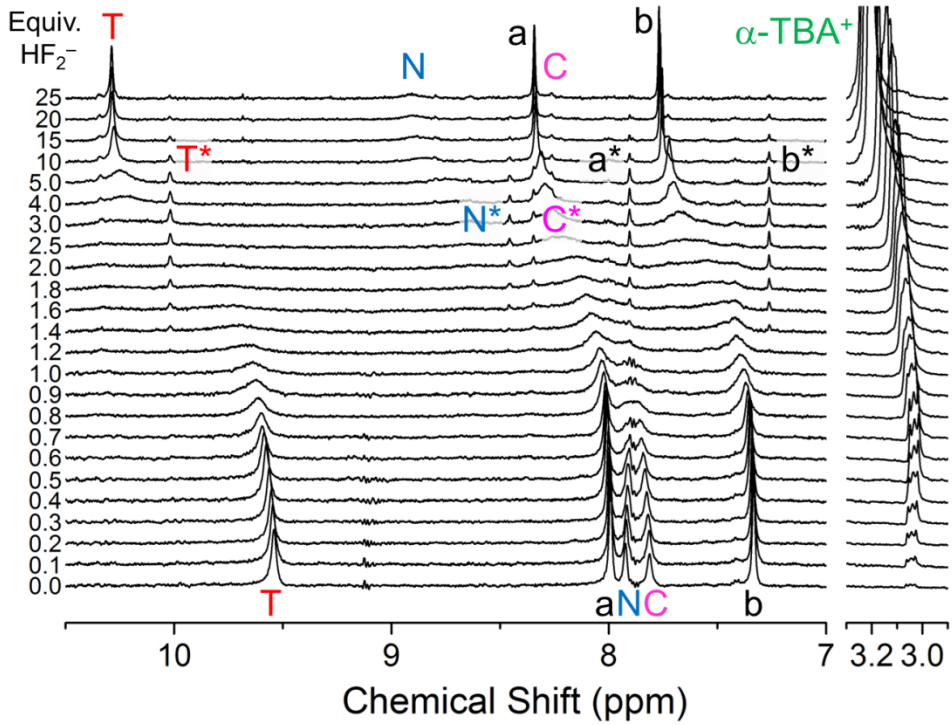

Figure S1. ^{1}H NMR titration of macrocycle **1** (0.5 mM) in CD_2Cl_2 with $TBAHF_2$ (500 MHz, 298 K).

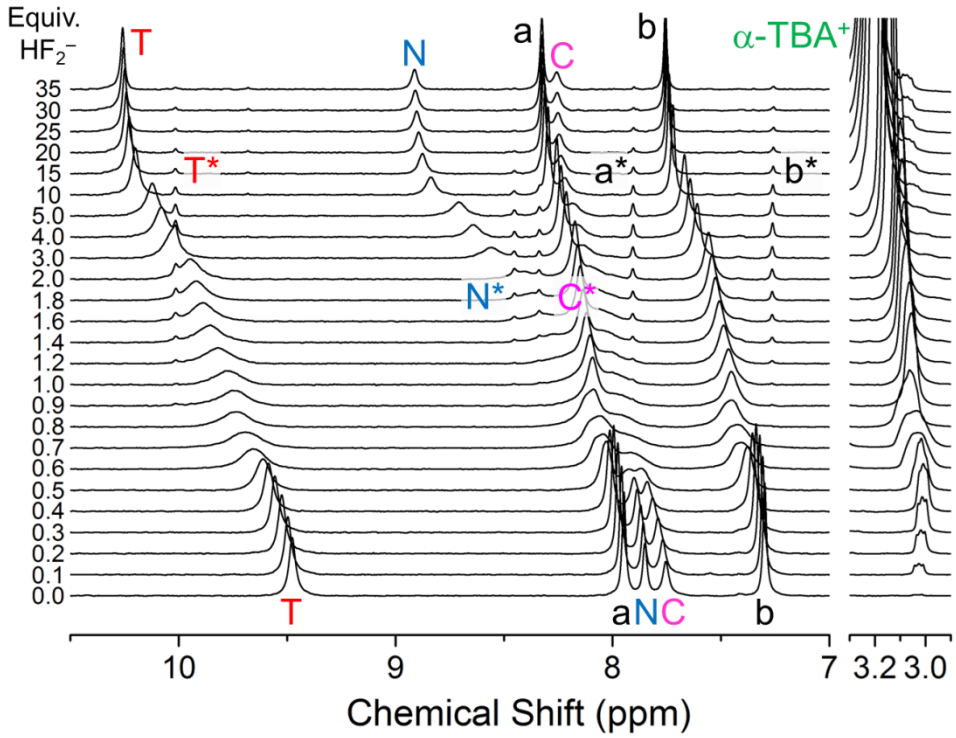

Figure S2. ^{1}H NMR titration of macrocycle **1** (2 mM) in CD_2Cl_2 with $TBAHF_2$ (500 MHz, 298 K).

S.4 CHARACTERIZATIONS OF FLUORINE SPECIES

Minor species (peaks noted with *) were observed in the ^{1}H NMR titrations of **1** with $TBAHF_2$ at two concentrations (0.5 and 2 mM). Even though the chemical shifts of the minor species did not change, the relative intensities reached a maximum when *ca.* 4 equivalents of $TBAHF_2$ was added and decreased upon adding excess $TBAHF_2$. This led to the hypothesis that the minor species present is correlated with the macrocycle **1** and bifluoride anion.

The organic component of the minor species has been characterized using diffusion NMR (*Figure S3*) and 2D EXSY/ROESY NMR (*Figure S4, S5*). Both of these experiments were carried out on an aged, 2 mM solution of **1** in CD_2Cl_2 with 4.0 equivalents of $TBAHF_2$.

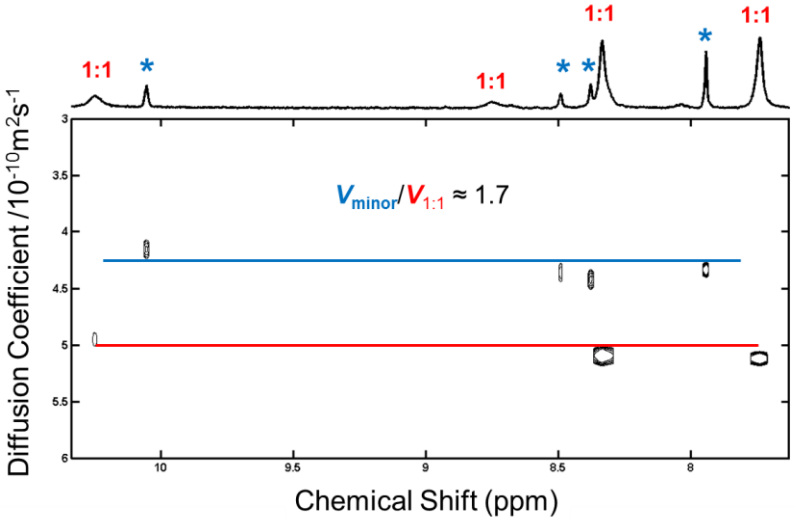

Figure S3. DOSY NMR of macrocycle **1** (2 mM) in CD_2Cl_2 with $TBAHF_2$ (500 MHz, 298 K).

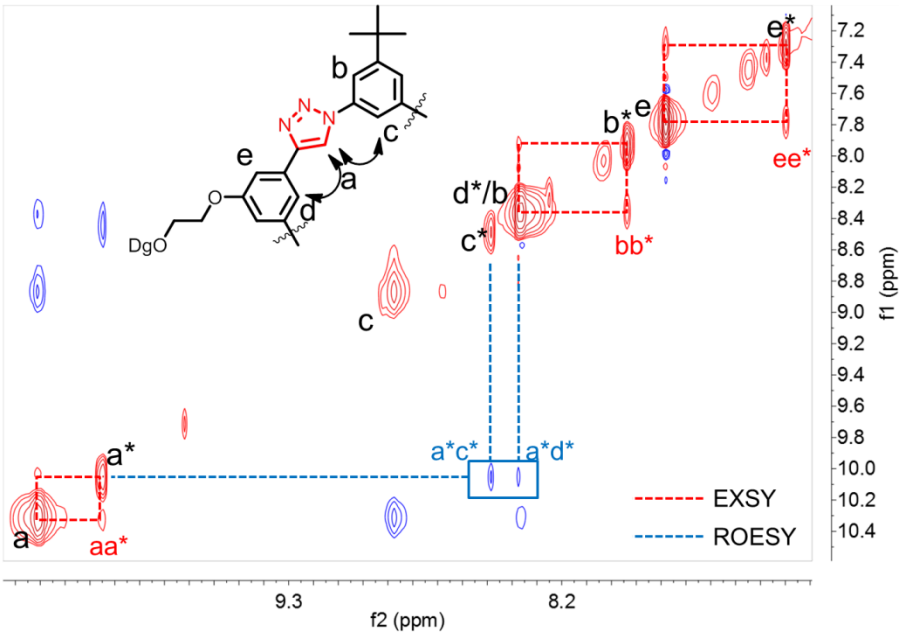

Figure S4. ^{1}H-^{1}H EXSY/ROESY NMR of macrocycle **1** (2 mM) in CD_2Cl_2 with $TBAHF_2$ (500 MHz, 298 K).

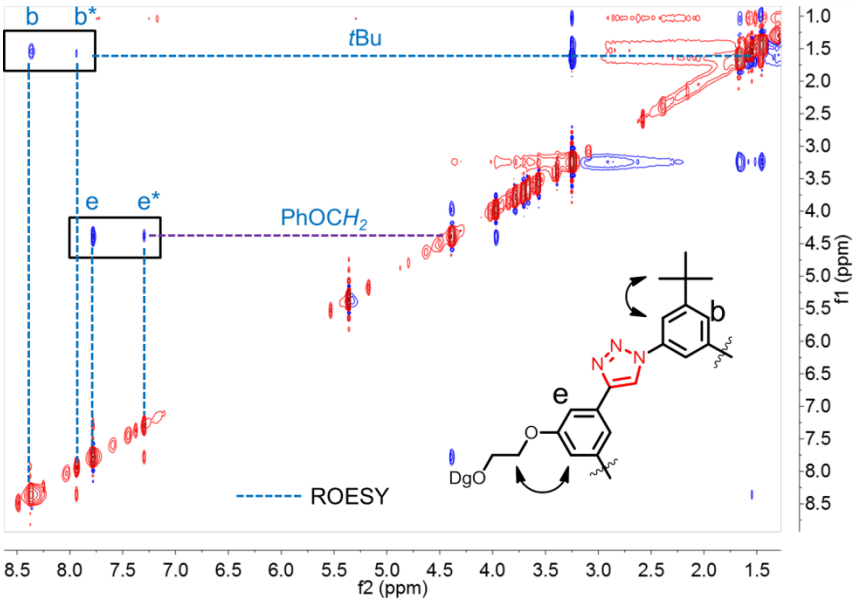

Figure S5. ^{1}H-^{1}H ROESY NMR of macrocycle **1** (2 mM) in CD_2Cl_2 with $TBAHF_2$ (500 MHz, 298 K).

The organic component of the minor species was concluded to be *a sandwich of two macrocycles of **1*** based on the following observations:

• Diffusion NMR (*Figure S3*) indicates that the minor species is twice the size of the 1:1 complex **1**•HF_2^-.

• EXSY/ROESY NMR (*Figure S4*) spectrum confirms that the organic component of the minor species is entirely comprised of **1** on account of the fact that all protons peaks associated with the minor species show cross peaks with macrocycle **1**.

• In the ^{1}H NMR spectra (*Figure S2*), the chemical shifts of proton peaks associated with the minor species are generally upfield compared to those in the 1:1 complex **1**•HF_2^-.

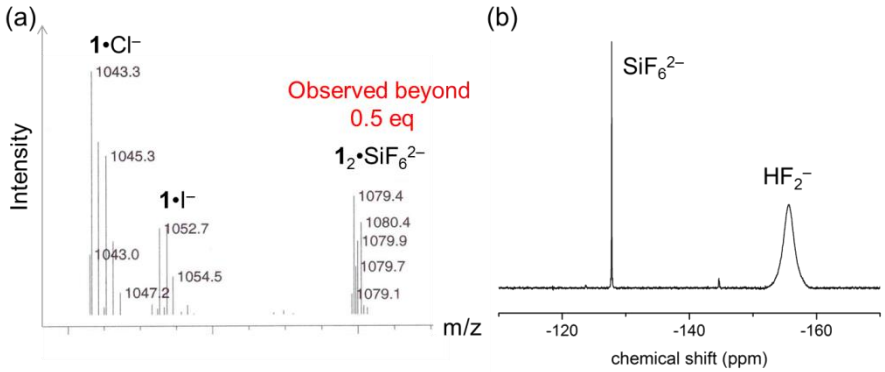

Figure S6. (a) Mass spectrometry found a dianionic species corresponding to $\mathbf{1}_2$•SiF_6^{2-}. (b) ^{19}F NMR of **1** with $TBAHF_2$ (400 MHz, 298 K, 0.8 M, CD_2Cl_2).

The anion that was sandwiched by $\mathbf{1}_2$ was confirmed to be SiF_6^{2-} based on mass spectrometry and ^{19}F NMR spectroscopy [S8] (*Figure S6*). The same complexation-induced chemical shifts (0.6 ppm) for *all* hydrogen bonded protons, *i.e.*, peaks T (9.5 ppm), N (8.9 ppm), and C (8.8 ppm) (*Figure S2*), also support the presence of this highly symmetric anion, The sample for mass spectrometry was prepared as a 1 mM solution in THF with 3.0 equivalents $TBAHF_2$. Chloride and iodide in the mass spectra were scavenged from the loop used in the instrument. The bifluoride complex cannot be observed in the mass spectra after multiple attempts. We note that fluoride and cyanide[S13] complexes of triazolophanes have not been observed either. These observations suggest that the high basicity of these anions (CN^- and F^-) and bifluoride's speciation to HF and F^-, allow loss of the anions as neutral gases HF and HCN from the gas phase mixture. Presumably, the solvent serves as a proton source.

This appearance of hexafluorosilicate, SiF_6^{2-}, was a result of bifluoride etching glass, which has been reported before.[S9] The SiF_6^{2-} is not stable in solution.[S10] The highest concentration was evaluated (*Figure S7*) by measuring ^{19}F NMR spectra of a 2 mM bifluoride solution in CD_2Cl_2, which had been aged for 2 h. On the basis of this experiment, the highest concentration of hexafluorosilicate that would be present during the quantitative titrations conducted at 0.5 or 5 μM as monitored by UV-Vis spectroscopy was determined to be 0.7 mol% of bifluoride. The experimental conditions of the ^{19}F NMR were based on the following points:

- During a quantitative UV-Vis titration, the most concentrated bifluoride solution should be the stock solution, which is 2 mM.
- A typical UV-Vis titration takes 2 h at most.
- When the bifluoride is bound to the macrocycle, it is not able to effectively etch glass on account of the fact that the 2:1 sandwich complex, $\mathbf{1}_2$•SiF_6^{2-}, was only observed in ^1H NMR titrations after 1 equivalent of bifluoride was added, i.e., when free bifluoride began to accumulate in solutions.

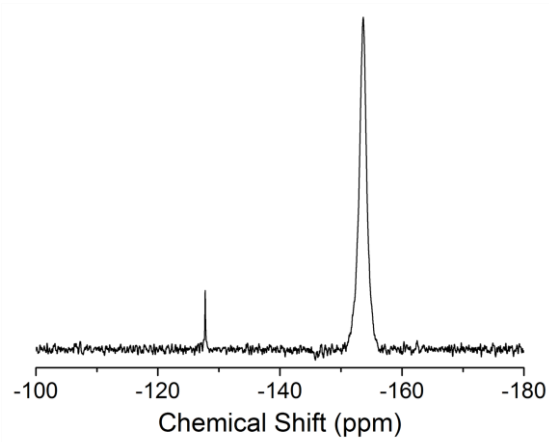

Figure S7. ^{19}F NMR spectrum of $TBAHF_2$ (400 MHz, 298 K, 2 mM, CD_2Cl_2).

The presence of the hexafluorosilicate dianion and the bifluoride anion are thus both expected to be present in studies involving the addition of F^- ions. Herein, we provide the ^{19}F NMR spectra of SiF_6^{2-} and HF_2^- in different deuterated solvents as references for related studies, such as anion

binding and sensing of fluoride and bifluoride. The chemical shift of both species is sensitive to solvent polarity. As the polarity increases, the hydrogen bond strength in HF_2^- decreases and gives rise to a continuous shift to upfield positions.

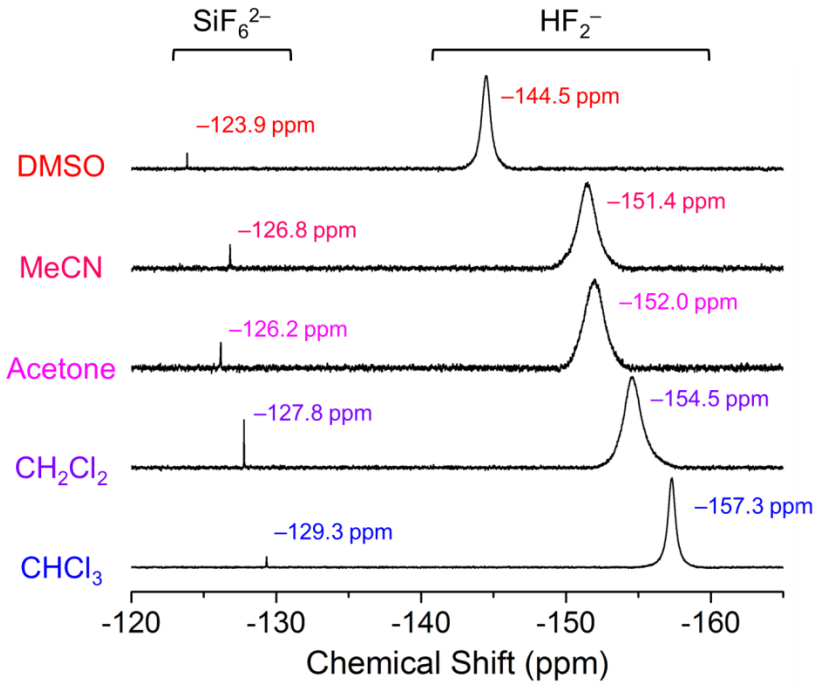

Figure S8. ^{19}F NMR spectra of $TBAHF_2$ in different solvents (400 MHz, 298 K, 10 mM).

We surveyed ~30 literature publications over the past 10 years and found that bifluoride and hexafluorosilicate are mentioned infrequently. The peak broadening associated with bifluoride can cause trouble when identifying the fluorine signals. When conducting qualitative analyses, we believe that the presence of these species is less likely to impact the conclusions that have been drawn in those papers regarding the impact of added fluoride on observed spectroscopic changes. However, in quantitative studies, omission of SiF_6^{2-} and HF_2^- will likely lead to large errors when providing a basis for understanding anion selectivities.

S.5 ION PAIR DETERMINATION OF TETRABUTYLAMMONIUM BIFLUORIDE

The ion-pair association constant (K_{ip}) for $TBAHF_2$ had not been determined previously. In addition, $TBAHF_2$ does not absorb light in the region around 230–260 nm. To quantify K_{ip}, a variable concentration NMR study was conducted instead of UV-Vis spectroscopy. CD_2Cl_2 (400 μL) was prepared in a screw-cap NMR tube equipped with PTFE/silicone septa. Aliquots of 2 mM $TBAHF_2$ solutions in screw-cap vials equipped with PTFE/silicone septa were added using 10 μL and 100 μL gas-tight micro-syringes. The water present in the solutions (1.5 ppm) was confirmed to be innocent in this study on account of the fact that a parallel titration, in which the water was different, gave the same fitting result within error. However, because of the overlap with the water peak, two flanking protons (β and γ) were excluded from data fitting.

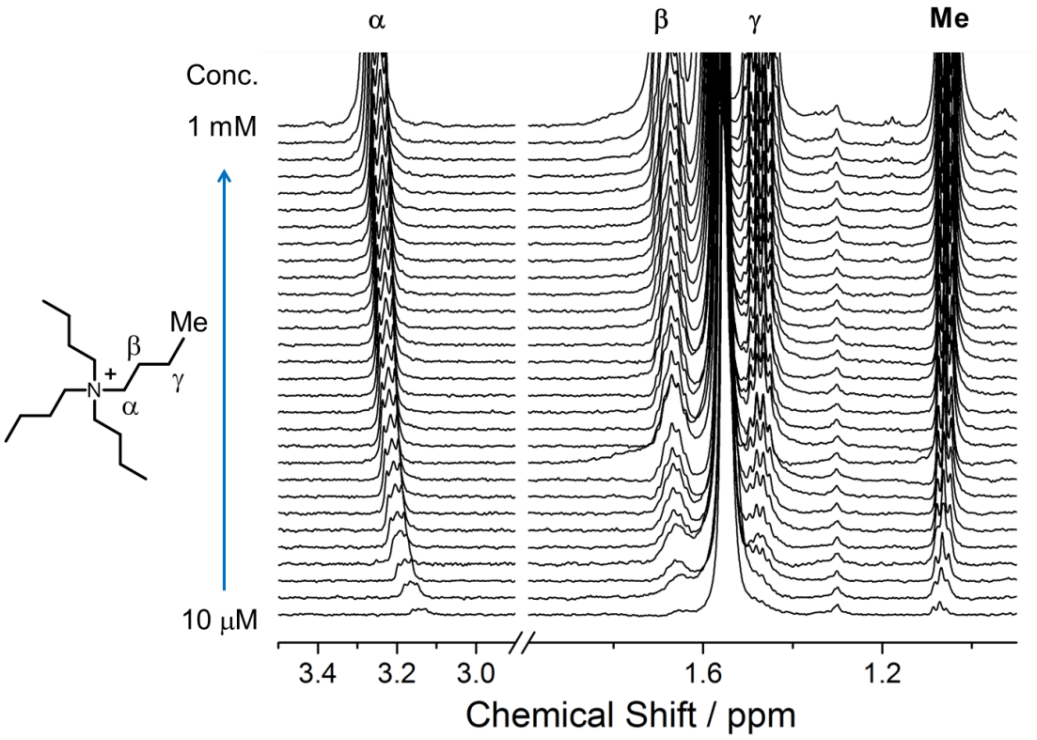

Figure S9. Variable concentration ^{1}H NMR of $TBAHF_2$ (500 MHz, 298 K, CD_2Cl_2).

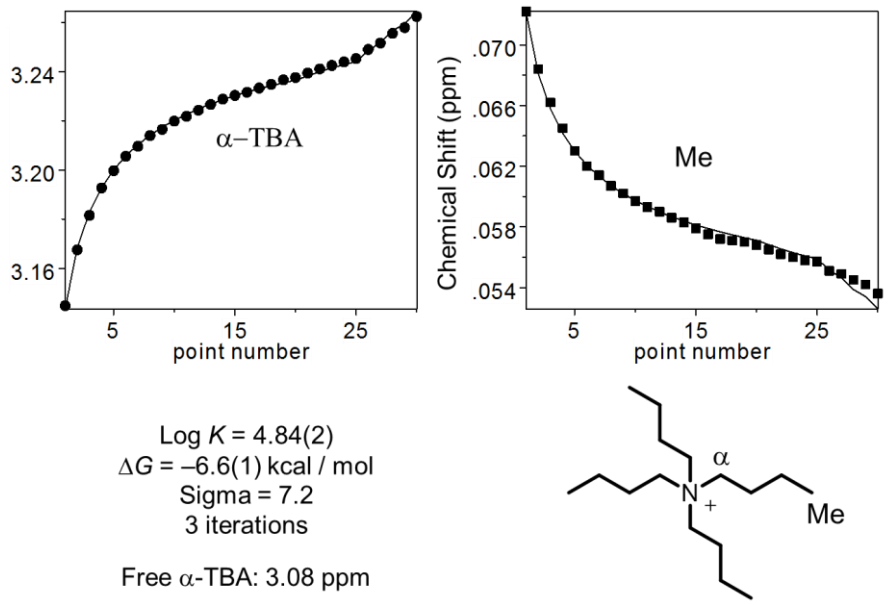

Figure S10. Data fitting result from HypNMR 2009.

Table S1. K_{ip} of TBACl[11] and $TBAHF_2$

Salt	TBACl	$TBAHF_2$
K_{ip}	4.85 ±0.02	4.84 ±0.02

S.6 VARIABLE CONCENTRATION ^{1}H NMR STUDIES OF TBA•1_2•HF_2

At millimolar concentrations, we have shown[S12] previously that a macrocyclic complex with a bound anion can interact further with the countercation in dichloromethane to form an ion-pair complex. When the charged 1:1 host:guest complex forms a neutral ion-pair complex, a turning point in the chemical shift changes that follows anion addition was observed[S12] for the α-TBA proton instead of monotonic changes expected for a simple two-component equilibrium. This behavior arises when the dominating equilibrium shifts from those associated with the free TBA^+ and TBACl to those equilibria involving exchange of the TBA^+ between TBACl and the ion-pair complex. This turning point was seen[S12] at around 1.0 equivalent of added TBACl corresponding to the situation when the relative concentration of the 1:1 host-guest complex first approaches its maximum.

However, if a turning point is observed when only 0.5 equivalent of anion is added, a different ion-pair complex is anticipated: a 2:1 sandwich complex (**1**$_2$•HF_2) that is interacting with the counteraction TBA^+. This is the observation made with $TBAHF_2$. At 2 mM (*Figure S11*), the α-TBA^+ signal starts at an upfield position compared to the free TBA^+ indicating TBA^+ is ion-paired. Typically, a 2:1 sandwich complex reaches its maximum population at around 0.5 equivalent and then, because of mass actions, it dissociates into the 1:1 complex by adding more HF_2^-. The observed turning point coincides with the population changes of the 2:1 sandwich complex strongly indicating the existence of the 2:1 ion-pair complex (**1**$_2$•HF_2^-•TBA^+).

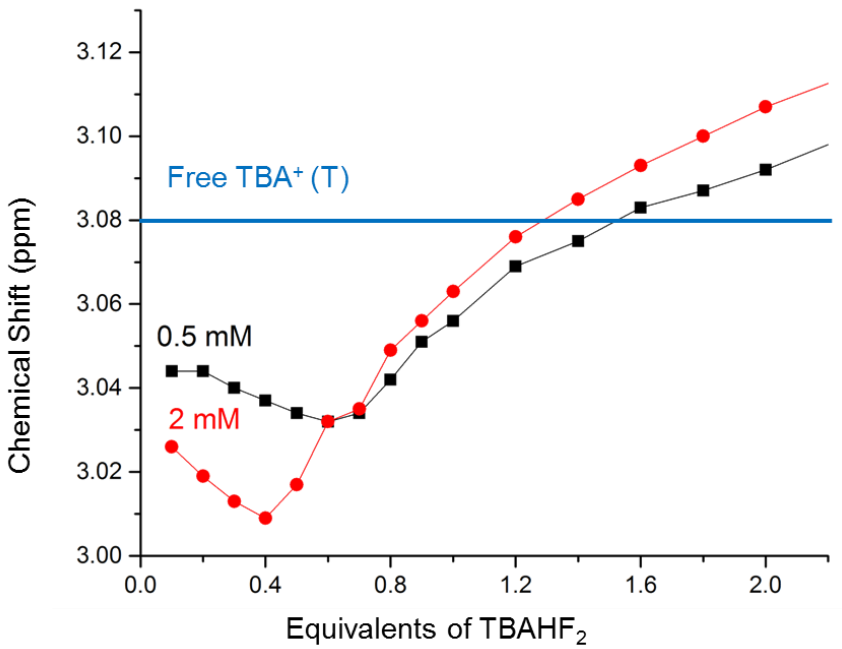

Figure S11. Chemical shift changes of α-TBA^+ proton at two different concentrations (0.5 and 2 mM, 500 MHz, 298 K, CD_2Cl_2).

To further confirm this assignment, diffusion NMR was not viable because the α-TBA^+ proton is a linear combination of all possible species in solutions: free TBA^+, TBACl, **1**•HF_2^-•TBA^+, **1**$_2$•HF_2^-•TBA^+. The error of measuring the diffusion coefficient of TBA^+ as well as the low fidelity of **1**$_2$•HF_2^-•TBA^+ rendered the chemical shift changes of α-TBA^+ the best probe to confirm the putative **1**$_2$•HF_2^-•TBA^+. We utilized the fact that a 2:1 complex is a higher order

species that can be destabilized when the solution is diluted. Therefore, ^{1}H NMR titration at 0.5 mM was conducted.

At this concentration, the turning point shifted towards 1.0 equivalent, which indicates the formation and greater population of **1**•HF_2^-•TBA^+ in solution. Interestingly, the major differences of chemical shift changes in the α-TBA^+ peak the between two concentrations are those below 0.6 equivalent. This situation is consistent with the α-TBA^+ protons being more shielded in a 2:1 ion-pair complex than in the 1:1 ion-pair complex. Overall, this experiment corroborated the presence of the $\mathbf{1}_2$•HF_2^-•TBA^+ in solution in addition to the 1:1:1 type of ion-pair complex **1**•HF_2^-•TBA^+ we had seen before.[S12] Pairing of the countercation is related to the electron density of the complex. The fact that we only see evidence for this 2:1 ion pair species with HF_2^- but not from the Cl^--binding ^{1}H NMR titrations reported here or elsewhere[S1,S4b,S12] suggests that HF_2^-may orient more perpendicular to the planes of the two macrocycles and so becoming more exposed than a monoatomic halide.

S.7 COMPUTATIONAL RESULT OF 3•HF_2^-

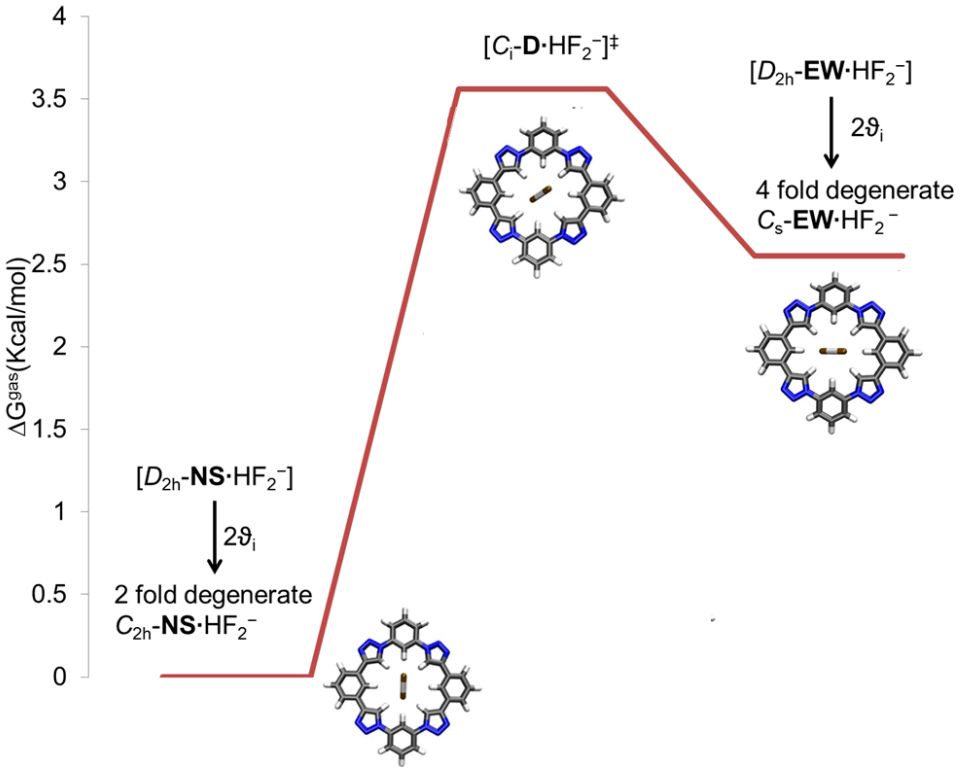

Figure S12. Free energy (kcal / mol) profile for all computed states. Geometry optimization was performed at M06-2X/6-31+G(d,p) and energies obtained at M06-2X/6-311++G(3df,2p).

The calculations were performed according to the General Methods. In-plane rotation of the bound bifluoride anion was investigated in order to identify any possible states that may exist as saddle points and thus obtain the free energy profile shown in Figure S12. Frequency calculations were employed to confirm whether the resulting structure was sitting in a local minimum (no imaginary frequency) or at a transition state (1 imaginary frequency). Binding arrangements with

the HF_2^- anion pointing towards different sets of CH hydrogen bond donors were investigated on account of our previous studies with CN^-.[S13] Each structure was optimized starting from an initial idealized symmetry, *i.e.*, D_{2h} for the **N**orth-**S**outh and **E**ast-**W**est modes, and C_i for **D**iagonal modes (*Figure S12*). All other in-plane arrangements were found to converge to one of these three states indicating that we have obtained all the possible states.

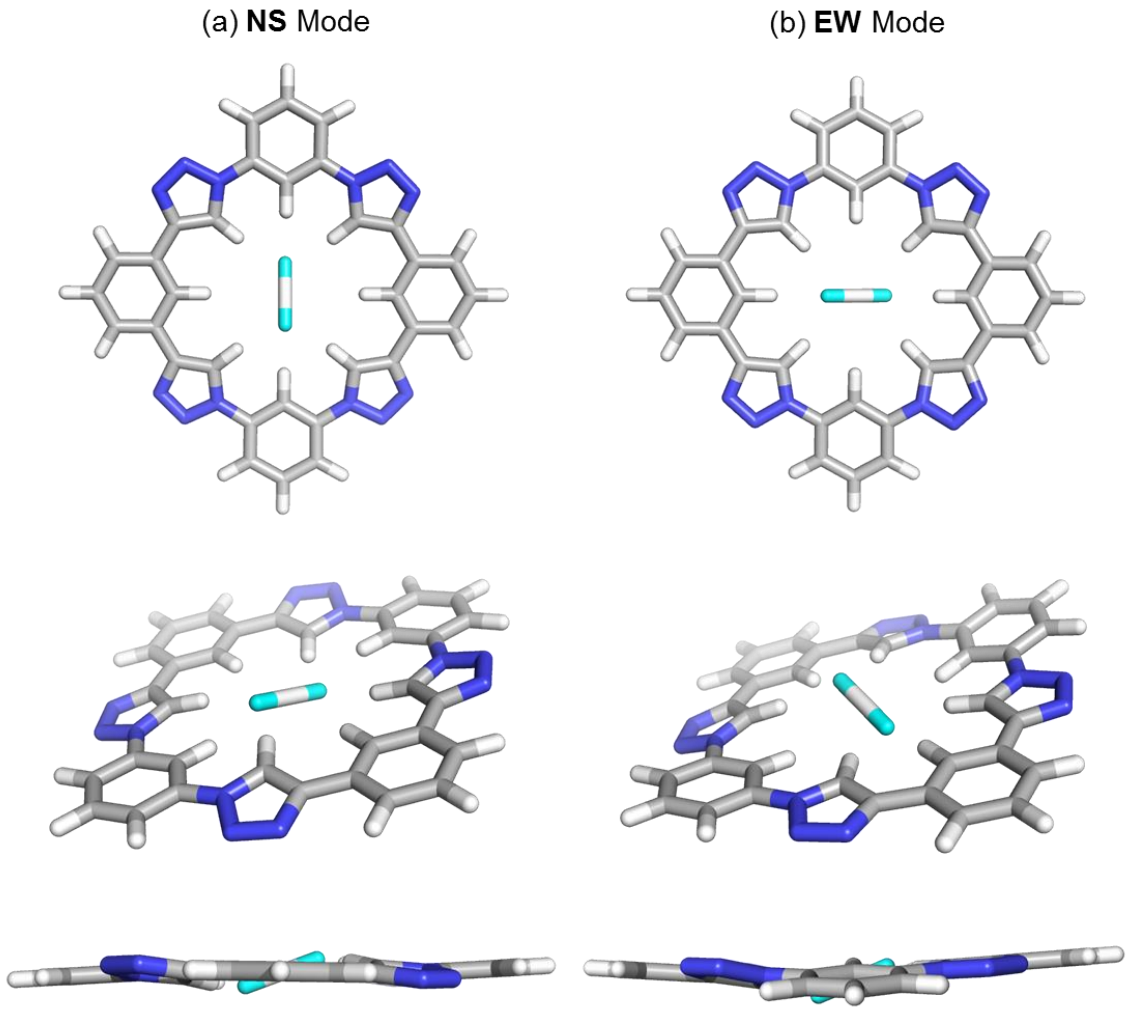

Figure S13. Two local minima computed for **3**•HF_2^-: (a) **NS** mode (b) **EW** mode in their top views, south-east views, and east-west side views.

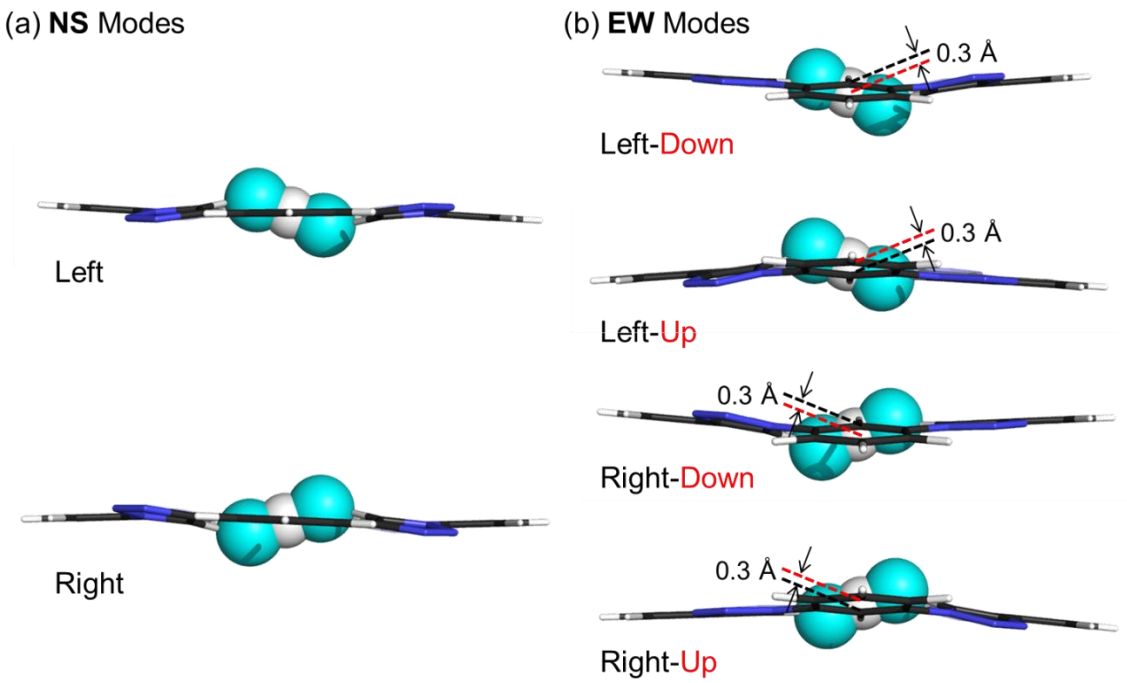

Figure S14. Degenerate states in the **NS** and **EW** binding modes: (a) Side view of the two **NS** modes in north-south side view and (b) four **EW** modes in east-west side view. In the **EW** mode, displacements of the bifluoride from the center of mass of triazolophane **3** is indicated.

***Table S2*.** Computed structural data for **3**•HF_2^- in the **NS** and **EW** modes.

Distances[a]	**NS**	**EW**[b]
F•••H^T	1.97	2.01, 2.02
F•••H^N	1.98	3.01, 3.14
F•••H^C	3.11	2.04, 2.05
C–H^T	1.085	1.085
C–H^N	1.085	1.085
C–H^C	1.088	1.086
H^T•••H^T	5.32	5.26
H^N•••H^N	5.95	5.66
H^C•••H^C	5.79	6.10
F–H	1.13	1.14[b], 1.12[c]
∠F–H–F	180°	179.2°
Tilting Angle[c]	21°	21°

(a) All distances are in Å. (b) For columns containing two values, the first value is corresponding to the closer half of bifluoride towards the center of the cavity. (c) The tilting angle is defined as the angle between the linear bifluoride and the mean plane of the macrocycle.

S.8 ANALYSIS OF THE BINDING MODES OF 1•HF_2^- IN SOLUTION

Boltzmann Difference Between NS and EW Binding Modes:

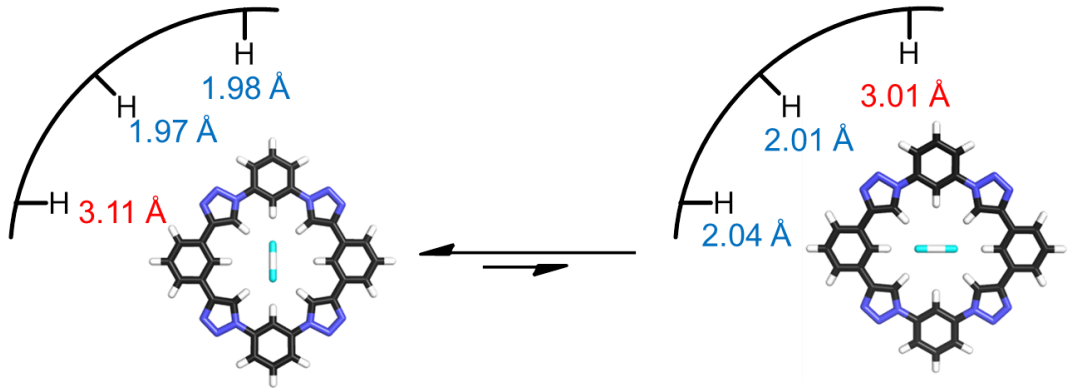

Figure S15. Hydrogen bond distances in the **NS** and **EW** states.

The calculation of the population difference between the **NS** and **EW** states in solution can be estimated from chemical shift positions. The observed chemical shift of a phenylene proton is a Boltzmann-weighted distribution (P) of the complexation-induced chemical shifts ($\Delta\delta_i$) in the **NS** and **EW** modes for protons H^N and H^C, respectively:

$$H^N: \Delta\delta_N * P_{NS} + \Delta\delta_N' * P_{EW} = 1.1 \text{ ppm} \quad \text{(S1)}$$

$$H^C: \Delta\delta_C' * P_{NS} + \Delta\delta_C * P_{EW} = 0.5 \text{ ppm} \quad \text{(S2)}$$

Where $\Delta\delta_N$ and $\Delta\delta_C$ are the chemical shifts induced by short H-bonded contacts; and $\Delta\delta_N'$ and $\Delta\delta_N'$ are from the long contacts. The sum of the distribution between the **NS** and **EW** modes is 1:

$$P_{NS} + P_{EW} = 1 \quad \text{(S3)}$$

On account of the fact that H-bonded distances are the same to within 3% for the bifluoride bound into the north-south ends of the cavity in the **NS** mode as for the bifluoride into the east-west ends of the cavity in the **EW** mode, the analysis can be simplified. Consequently, we assume the complexation-induced chemical shifts of phenylene protons involved in short contacts are the same in both the **NS** and **EW** arrangement, *i.e.*, $\Delta\delta_N = \Delta\delta_C$. The same reasoning applies for the long contacts, $\Delta\delta_N' = \Delta\delta_C'$. Hitherto, there are four variables, P_N, P_C, $\Delta\delta_N$ and $\Delta\delta_N'$, in three equations obtained above. In order to solve these equations, the shifts, $\Delta\delta_N'$, involved in long contacts, are assumed to be 0 on account of the fact that its hydrogen bond distances (3 Å) are larger than the sum of the van der Waals radii of fluorine and hydrogen atoms (2.7 Å). Subsequently, the distributions for two modes in solution can be solved:

$$P_{NS} = 0.74,\ P_{EW} = 0.26 \quad \text{(S4)}$$

The free energy differences are calculated using the Boltzmann equation taking into account the degeneracies: 2 for **NS** and 4 for **EW** (*vide supra*):

$$4P_{NS} / 2P_{EW} = \exp(-\Delta G_{sol} / k_B T) \quad \text{(S5)}$$

$$\Delta G_{sol} = 1.0 \text{ kcal mol}^{-1} \quad \text{(S6)}$$

To evaluate the error introduced by the assumption that the complexation-induced chemical shift of the protons involved in the long contacts ($\Delta\delta_N$' and $\Delta\delta_C$') is 0 ppm, this chemical shift value was varied (*Table S3*). The range (0–0.14 ppm) is obtained by examining shifts of non-hydrogen-bonded protons in F^- titrations performed previously, which displayed ~0.1 ppm shifts.[S1] In addition, these values are consistent with the observed chemical shift of the non-hydrogen-bonded proton (H^N) during the titration of $TBAHF_2$ with **2** (*vide supra*).

Table S3. Error analysis of calculation of the population difference between of the **NS** and **EW** states of 1:1 bifluoride complex **1**•HF_2^- (298 K, CD_2Cl_2).

$\Delta\delta_N$' (ppm)	$\Delta\delta_N$ (ppm)	N_C	N_N	$\Delta\Delta G_{soln}$ (kcal mol^{-1})
0	1.60	0.31	0.69	0.9
0.02	1.58	0.30	0.70	0.9
0.06	1.54	0.28	0.72	1.0
0.10	1.50	0.26	0.74	1.0
0.14	1.46	0.23	0.77	1.1

Broad H-Bonded Proton Peaks with HF_2^- Saturation:

The protons that form H-bonds with the bifluoride are broader than expected. The FWHM (full width at half maximum) evaluates the peak width of a proton signal in the ^{1}H NMR spectra. It is also a good indicator of the proton's involvement in dynamic exchange processes (conformational and equilibriation). In particular, this information is embedded in their own natural line width when the protons are undergoing fast exchange. Herein, we compare the FWHM of the free macrocycle **1** to the saturated 1:1 complexes between **1** and anions. In general, free macrocycles show a small degree of self-association at mM concentrations.[S1] When anions are bound, deaggregation occurs. Binding an anion would lower conformational freedom of these rigid, shape-persistent macrocycles. Consequently, a decrease in FWHM would be expected when a macrocycle binds an anion and reaches its thermodynamically most stable form. This behavior is what we observed for halides [S1] and cyanide (*Table S4*).[S13] When the FWHM increases, other factors must be playing a role. Strong coupling between fluorine atoms from the bifluoride anion and hydrogen atoms from the C–H donors can be attributed to line width

changes. However, we did not observe such a coupling in the ^{19}F NMR spectra even at low temperature (223 K) where the exchange rates are slow enough to allow for better resolution of peaks. One possibility for broadening is the existence of dynamic exchange between the **NS** and **EW** modes. The peak broadening could thus be explained by changes of their electronic environment, *e.g.*, hydrogen bonding protons, during the precession of bifluoride. Alternatively, if the anion binding and release were to account for this observation, we would also expect to see it with **1**•Cl^- and **1**•Br^-, yet we do not. We note that Bowman-James's bifluoride cage[S14] displays broad NH-based H-bonded peaks. Thus, we cannot exclude other types of exchange phenomena.

Table S4. Full width at half maximum (FWHM)[a] for all aromatic protons of triazolophane **1** (2 mM, CH_2Cl_2, 298 K) before and after adding bifluoride.

Protons	H^T	H^N	H^C	$CHDCl_2$
1	15	9	13.5	5
1•Cl^{-b}	4	8.5	6.5	3
1•Br^{-b}	3.5	7	6.5	3
1•HF_2^-	8	13	16.5	3.5

(a) All peak widths are in Hz. (b) Data from reference 1 is used for comparison.

S.9 UV-VIS TITRATIONS OF MACROCYCLE 1 WITH BIFLUORIDE AND CHLORIDE

Titrations were monitored on a Varian Cary 5000 UV-Vis-NIR spectrophotometer at room temperature (298 K). 4 mL of dilute host solutions (*e.g.*, 0.5 μM) were prepared in a 1 cm screw-cap quartz cell equipped with PTFE/silicone septa. Aliquots of concentrated TBA salt solutions (*e.g.*, 1 mM) in a screw-cap vial equipped with PTFE/silicone septa were added using 10 μL and 100 μL gas-tight micro-syringes.

Data analyses were conducted in Sivvu™ in the following manner:4

- Whole range of the spectrum for **1**, *i.e.*, 250–340 nm, was used for fitting.

- Corresponding equilibria from the predetermined binding model were included; the complete models and the model for UV-Vis titrations are discussed in the main text.

- Error analyses were generated by randomly ignoring 20% of the total data points (see associated table located below each fitted data sections).

The fitted data are presented in a square matrix of four components: (a) Top-left: raw titration data; (b) Top-right: simulated molar absorptivity; (c) Bottom-left: concentration profiles with equilibrium constants; (d) Bottom-right: RMS residuals (z axis) for fitted wavelengths (x axis) and solutions (y axis).

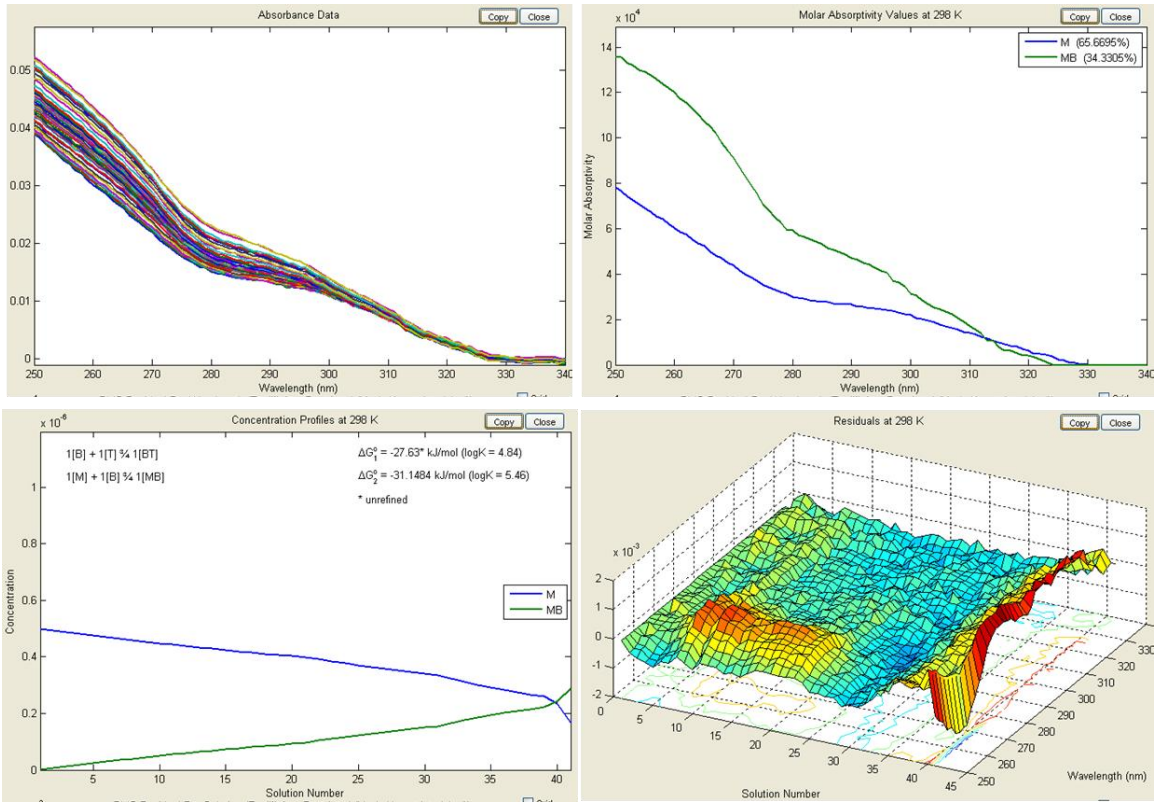

Figure S16. UV-Vis titration analysis of 1:1 complexation of **1** (0.5 μM) with $TBAHF_2$ (0–20 equivalents) in dichloromethane.

Dichloromethane Random Data Exclusion	K_1 **1** + HF_2^- ⇌ **1**•HF_2^-	K_{ip} $TBA^+ + HF_2^- \rightleftharpoons TBAHF_2$
None	5.46	Fixed
4 8 11 12 16 21 33	5.44	
2 6 12 15 18 26 30	5.46	
18 21 26 29 31 37 38	5.48	
3 7 8 15 16 24 29	5.46	
5 11 15 17 24 29 37	5.46	
6 7 13 27 31 32 38	5.47	
5 6 8 14 21 33 38	5.45	
Average	5.46 ± 0.01	4.84

Fitting Summary: RMS Residual: 0.0004; Data Reconstruction: 96.54%; Remaining Error Imbedded in Absorbance Values: 0.01%; R^2: 99.90%

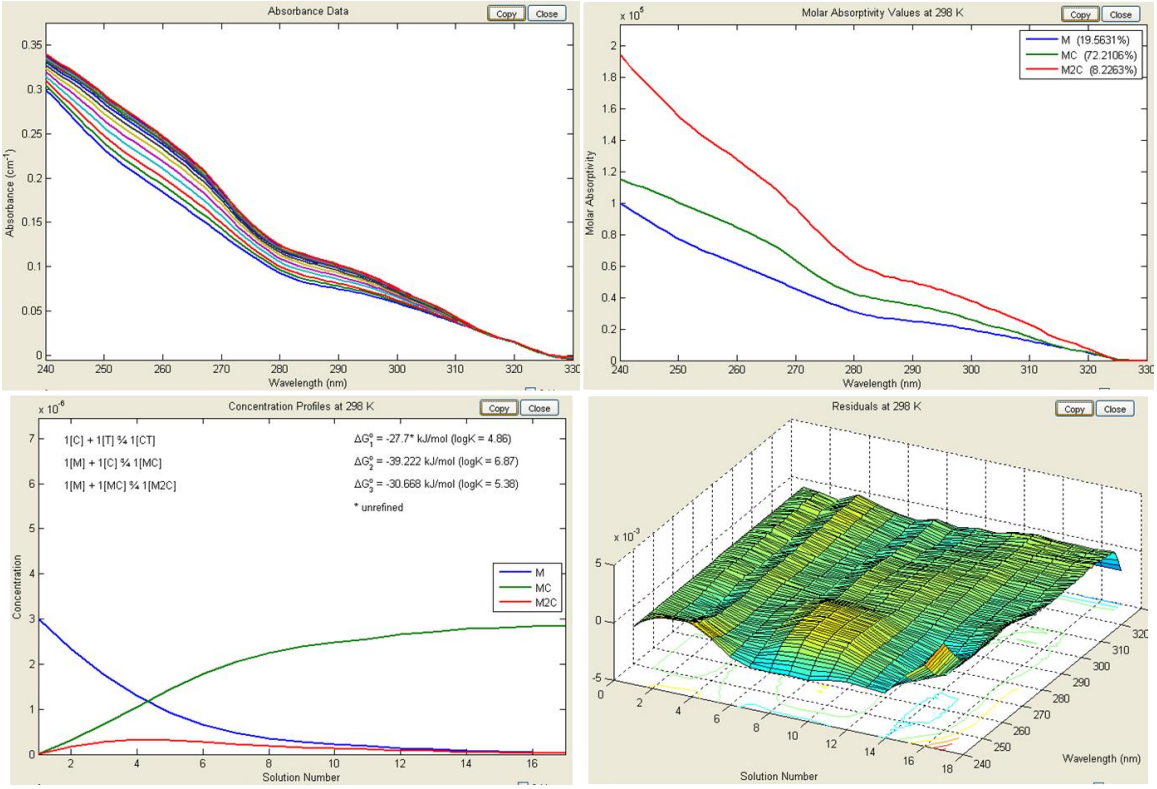

Figure S17. UV-Vis titration analysis of 1:1 complexation of **1** (3 μM) with TBACl (0–8 equivalents) in dichloromethane.

Dichloromethane	K_1	K_{ip}
Random Data Exclusion	**1** + Cl^- ⇌ **1**•Cl^-	TBA^+ + Cl^- ⇌ TBACl
None	6.87	Fixed
10 11 15	6.92	
2 5 14	6.87	
3 6 9	6.91	
7 9 12	6.90	
6 12 17	6.82	
3 7 11	6.89	
8 13 14	6.81	
Average	6.87 ± 0.04	4.85

Fitting Summary: RMS Residual: 0.0007; Data Reconstruction: 99.66%; Remaining Error Imbedded in Absorbance Values: 0.0003%; R^2: 99.995%

S.10 SPECIATION CURVES OF MACROCYCLE 1

The speciation curves were generated using Hyss2009[S15] using equilibrium constants determined analysis of the UV-Vis titration and utilizing ones estimated with the aid of NMR titrations according to the following observations:

• $\mathbf{1}_2$•HF_2^-•TBA^+ reaches 56% relative concentration at 0.5 equivalent. This population can be evaluated by the integrations of a pair of slow exchanging terminal methyl groups (Me) of the glycol chains that are associated with the 1:1 and 2:1 complexes at 3.4 ppm (*Figure S18*).

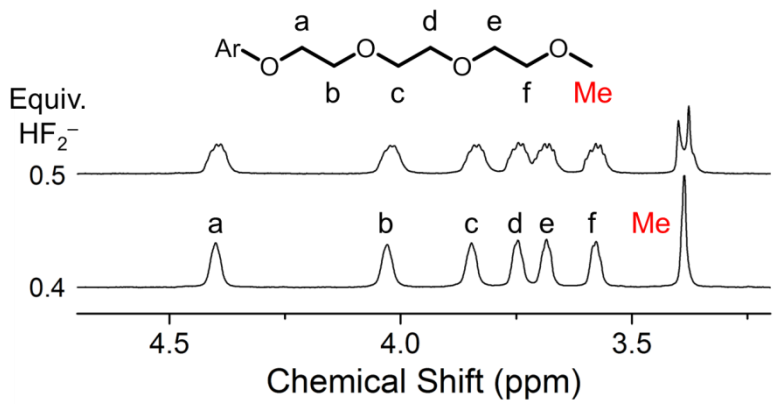

Figure S18. The glycol region of the ^{1}H NMR titration of macrocycle **1** (2 mM) in CD_2Cl_2 with $TBAHF_2$ (500 MHz, 298 K).

• $\mathbf{1}_2$•SiF_6^{2-} reaches 9% relative concentration at its maximum when 4 equivalents bifluoride anion was added. The percentage was determined using peak integrations of proton b at 7.5 ppm to its counterpartner in $\mathbf{1}_2$•SiF_6^{2-} at 7.2 ppm (*Figure S2*).

• Proton peaks are the broadest when *ca*. 2 equivalents bifluoride anion was added on account of the fact that the most number of species are in equilibrium with each other (*Figure S1*, *S2*).

• Two equilibria allow for the formation of $\mathbf{1}_2$•HF_2^-•TBA^+. These are the 2:1 formation and the ion-pair complex formation, which are shown below:

$$\mathbf{1}\bullet HF_2^- + \mathbf{1} \rightleftharpoons \mathbf{1}_2\bullet HF_2^- \qquad \text{(S7)}$$

$$\mathbf{1}_2\bullet HF_2^- + TBA^+ \rightleftharpoons \mathbf{1}_2\bullet HF_2^-\bullet TBA^+ \qquad \text{(S8)}$$

$$\mathbf{1}\bullet HF_2^- + \mathbf{1} + TBA^+ \rightleftharpoons \mathbf{1}_2\bullet HF_2^-\bullet TBA^+ \qquad \text{(S9)}$$

However, no NMR evidence can be found to identify the position of equilibrium for reactions S7 and S8. As a means to generate the speciation curves, the apparent formation constants of these

equilibria are evaluated–see reaction S9. Thus, the speciation curves (*Figure S19*, green trace) reflect both possible 2:1 species and we cannot discern the ratio of the 2:1 sandwich from its ion-pair complex. The same reasoning applies for $\mathbf{1}_2$•SiF_6^{2-} where the formation of **1**•SiF_6^{2-} cannot be distinguished from the dominating sandwich complex $\mathbf{1}_2$•SiF_6^{2-}. All the equilibrium constants are summarized in *Table S5*.

Table S5. Equilibrium constants associated with **1** binding HF_2^- (dichloromethane, 298 K) simulated in Figure S19.

Complexes	β [a]	Analysis Method	Method of Error Generation
1•HF_2^-	5.46 ±0.01	UV-Vis (0.5 μM)	Sivvu
1•HF_2^-•TBA^+	9.6 ±0.1	NMR (2 mM)	Hyss
$TBAHF_2$	4.84 ±0.2	UV-Vis (0.5 μM)	Sivvu
($\mathbf{1}_2$•HF_2^-•TBA^+ + $\mathbf{1}_2$•HF_2^-)[b]	9.9 ±0.1	NMR (2 mM)	Hyss
($\mathbf{1}_2$•SiF_6^{2-} + **1**•SiF_6^{2-})[c]	11.0 ±0.1	NMR (2 mM)	Hyss

(a) The β values represent the overall formation constants. (b) Two equilibria (S7, S8) are simulated as one apparent, overall equilibrium (S9) leading to the formation of 2:1 ion-pair complex $\mathbf{1}_2$•HF_2^-•TBA^+. β = [$\mathbf{1}_2$•HF_2^-•TBA^+] / ([**1**]^2[TBA^+][HF_2^-]). (c) Two equilibria are simulated as one apparent equilibrium leading to the formation of 2:1 ion-pair complex $\mathbf{1}_2$•SiF_6^{2-}. β = [$\mathbf{1}_2$•SiF_6^{2-}] / ([**1**]^2[SiF_6^{2-}]).

At 0.5 μM (*Figure S19*), all higher order species are removed from the equilibria by dilution, thus validating the use of much simpler model equilibria in the analysis of the UV-Vis titration data of bifluoride anion in section **S.9.**

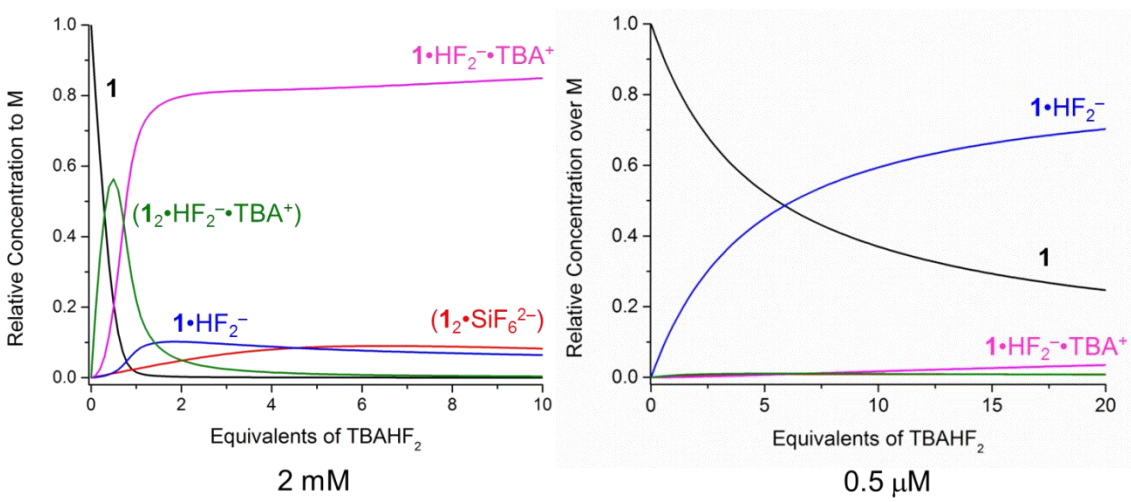

Figure S19. Speciation curve of **1** binding bifluoride in NMR and UV-Vis concentrations. $\mathbf{1}_2$•HF_2^-•TBA^+ and $\mathbf{1}_2$•HF_2^- is presented as ($\mathbf{1}_2$•HF_2^-•TBA^+) while **1**•SiF_6^{2-} and $\mathbf{1}_2$•SiF_6^{2-} is presented as ($\mathbf{1}_2$•SiF_6^{2-}). See Supporting Information text for more explanation.

S.11 COMPUTATIONAL RESULTS OF 5•HF_2^-, 6•HF_2^-, 4•HF_2^- & 4•Cl^-

The calculations were performed according to the General Methods. **EW** modes were explored in the virtual experiments by using computer-aided design on account of the fact that the cavity is expanded along this direction (*Table S4*). The bound bifluoride in any of the designed structures is expected to be less tilted in the **EW** mode than in the **NS** because of a shortening of the north-south axis. All the **EW** modes for bifluoride binding to **4**, **5**, and **6** are confirmed to be minima. Chloride complex was also investigated with **4** because of its ability to bind bifluoride with no tilting angle in **EW** mode.

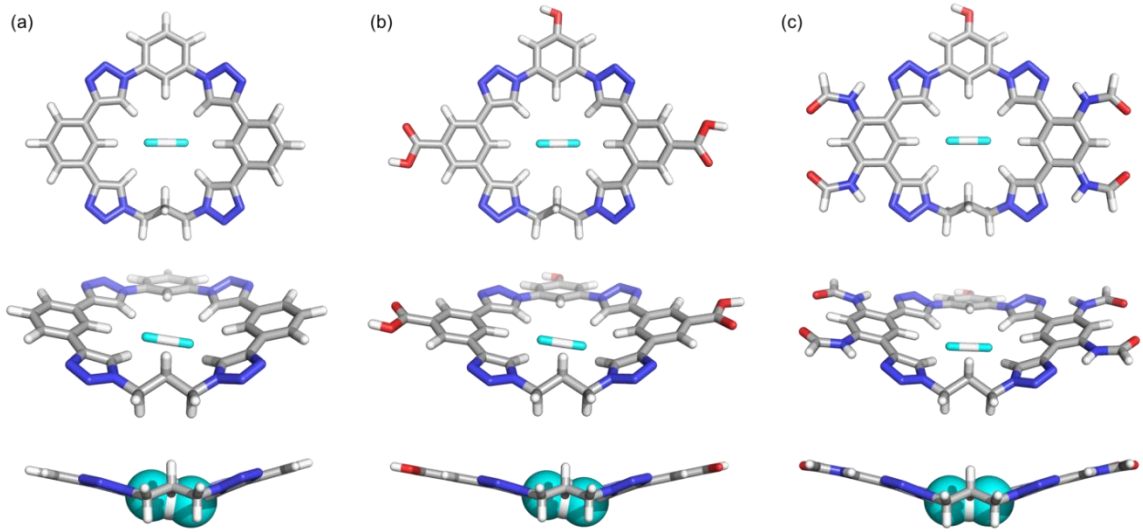

Figure S20. (a) **5**•HF_2^-, (b) **6**•HF_2^- and (c) **4**•HF_2^- in their top, perspective and side views.

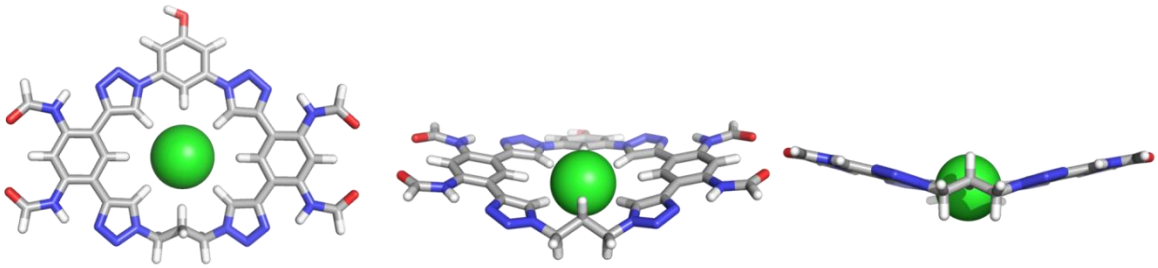

Figure S21. **4**•Cl^- in its top, perspective and side views.

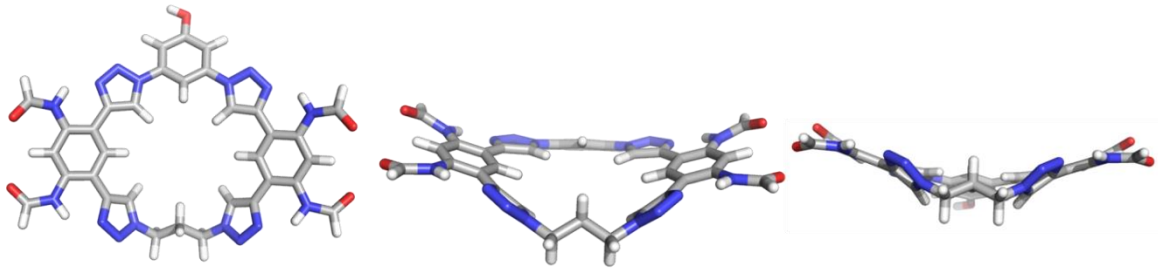

Figure S22. The empty form of triazolophane **4** in top, perspective and side views.

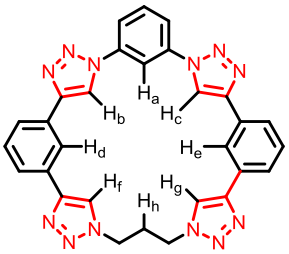

Figure S23. The generic structure of macrocycles computed in this section. The proton peaks are labeled so that a bound bifluoride in the **EW** mode has its left portion closer to the cavity.

Table S6. Computed structural data for **5**•HF_2^-, **6**•HF_2^- and **4**•HF_2^- in the **EW** modes and **4**•Cl^-.

Distances[a]	**5•HF_2^-**	**6•HF_2^-**	**4•HF_2^-**	**4•Cl^-**
F•••H_a[b]	3.10, 3.27	3.08, 3.22	3.12	2.82
F•••H_b	2.00	1.99	1.94	2.57
F•••H_c	2.03	2.02	1.95	2.58
F•••H_d	2.07	2.05	2.14	3.14
F•••H_e	2.08	2.06	2.14	3.14
F•••H_f	2.02	2.01	1.96	2.63
F•••H_g	2.02	2.02	1.96	2.63
F•••H_h	3.05, 3.10	3.04, 3.10	2.96, 2.97	2.81
C–H_a	1.085	1.084	1.085	1.087
C–H_b	1.086	1.086	1.086	1.086
C–H_c	1.086	1.086	1.086	1.086
C–H_d	1.086	1.087	1.086	1.087
C–H_e	1.087	1.087	1.086	1.087
C–H_f	1.086	1.085	1.086	1.086
C–H_g	1.086	1.086	1.086	1.086
C–H_h	1.096	1.096	1.096	1.097
F–H	1.14, 1.12	1.14, 1.12	1.13, 1.13	-
H_a•••H_h	5.72	5.71	5.54	5.60
H_b•••H_g	5.36	5.34	5.29	5.20
H_c•••H_f	5.30	5.31	5.31	5.21
H_d•••H_e	6.14	6.13	6.33	6.23
∠F–H–F	178.9°	179.0°	179.0°	-
Tilting Angle	10°	9°	0°	-

(a) All distances are in Å. (b) For columns containing two values, the first value corresponds to the closer half of bifluoride towards the center of the cavity.

S.12 ^{1}H NMR TITRATIONS OF MACROCYCLE 2

The titrations were performed in the same manner described in **S.3**. However, $CDCl_3$ was chosen instead of CD_2Cl_2 to improve the solubility of **2** while keeping the solvent properties similar.

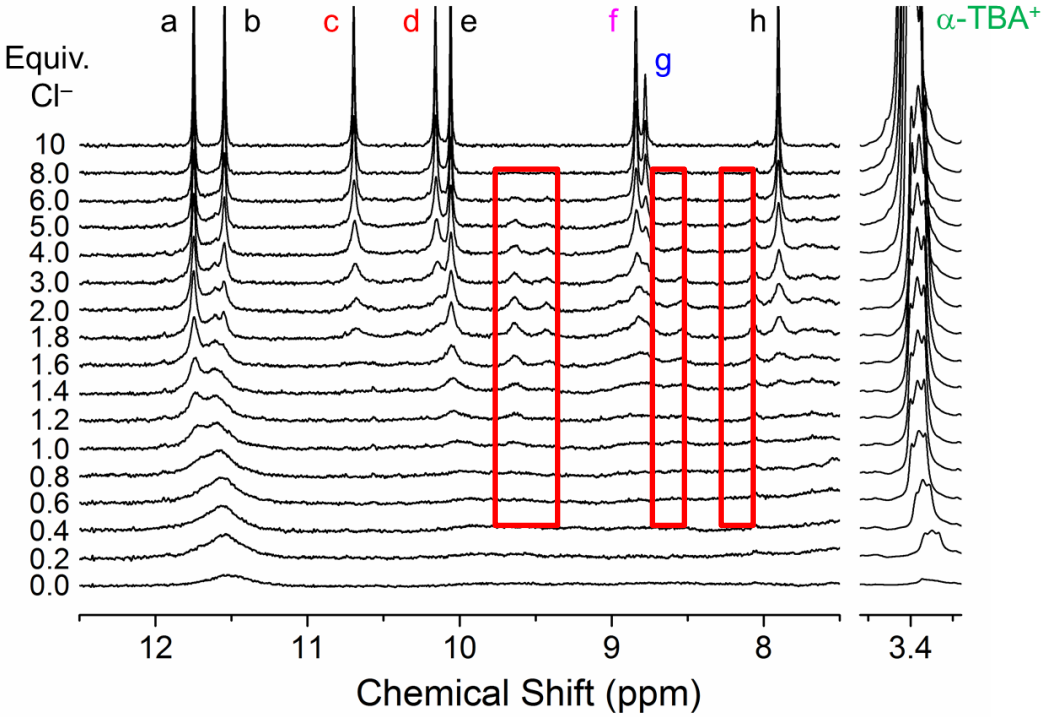

Figure S24. ^{1}H NMR titration of macrocycle **2** (2 mM) in $CDCl_3$ with TBACl (500 MHz, 298 K). Triazole protons are colored in red, north phenylene proton in blue, east-west phenylene protons in magenta. The red boxes indicate the presence of the 2:1 complex with Cl^-.

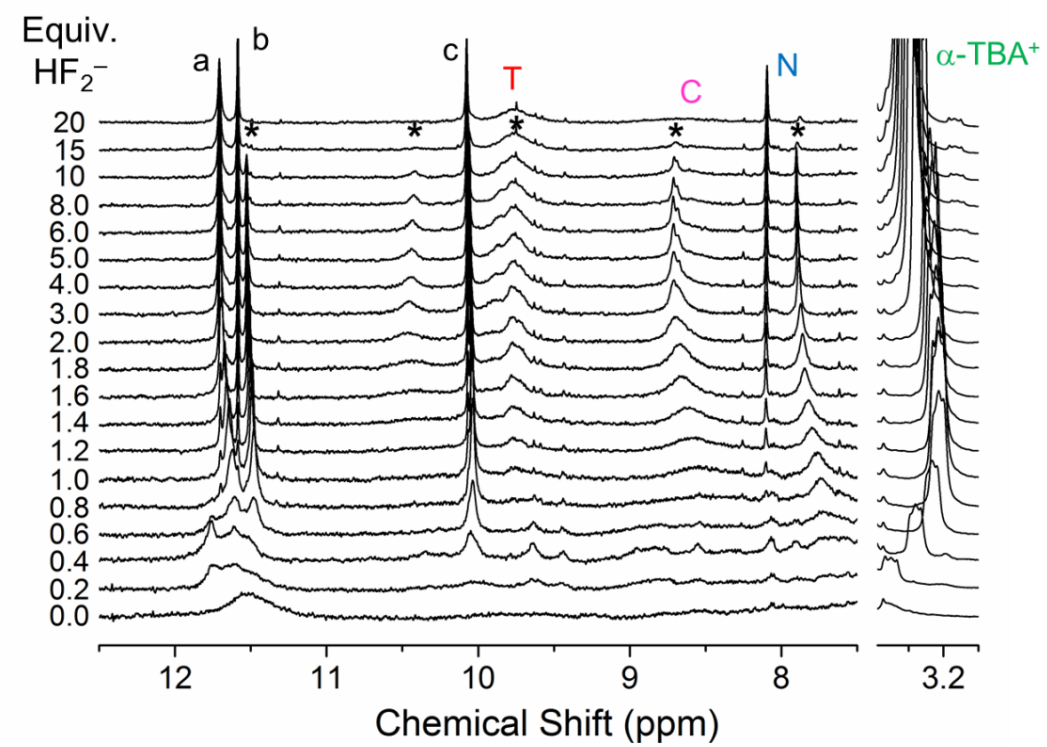

Figure S25. ^{1}H NMR titration of macrocycle **2** (2 mM) with $TBAHF_2$ ($CDCl_3$, 500 MHz, 298 K).

S.13 2D NMR CHRACTARIZARION OF 2•HF_2^- & 2•Cl^-

The proton patterns were very different between **2**•HF_2^- and **2**•Cl^-. 2D ROESY and ^{1}H-^{1}H TOCSY (**TO**tal **C**orrelation **S**pectroscop**Y**) were utilized to assign the protons in ^{1}H NMR.

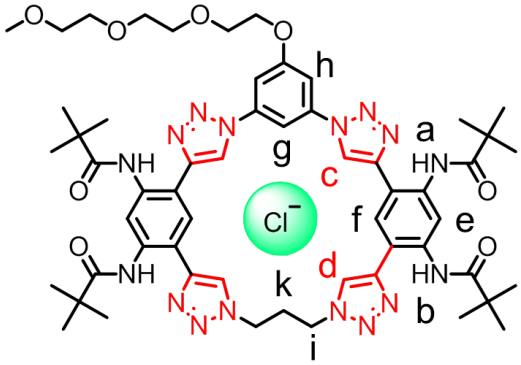

Figure S26. Summary of peak assignment for **2**•Cl^- in $CDCl_3$.

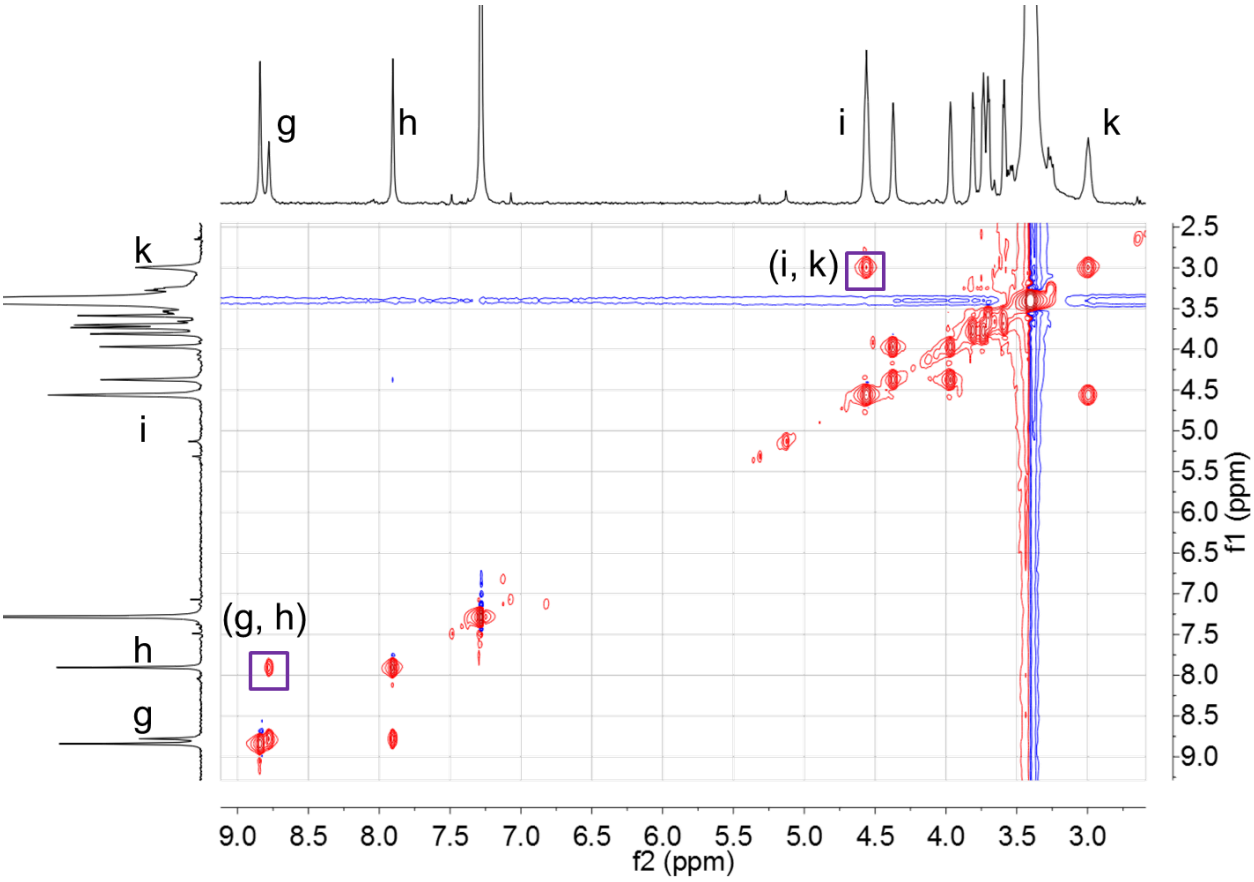

Figure S27. ^{1}H-^{1}H TOCSY NMR spectrum of macrocycle **2** (2 mM) in $CDCl_3$ with TBACl (500 MHz, 298K).

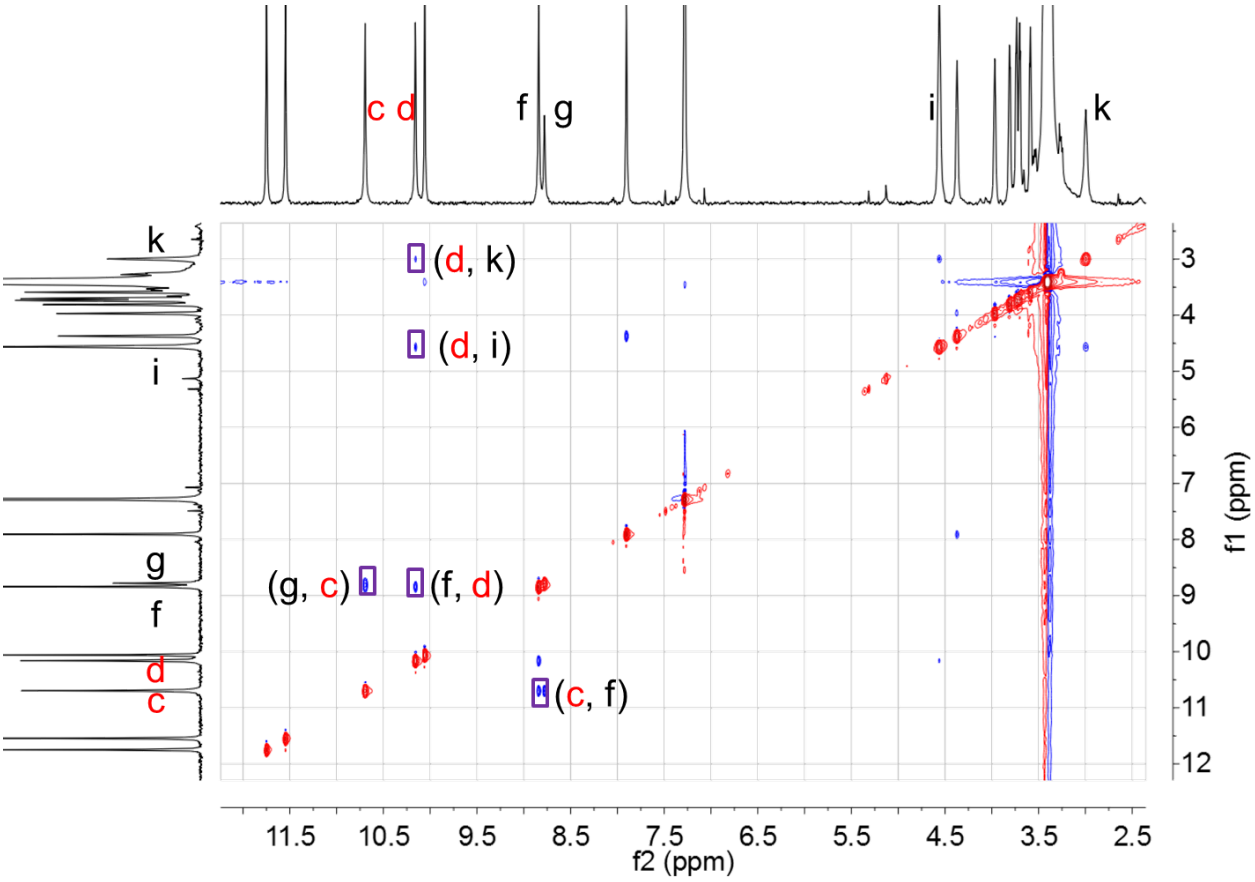

Figure S28. ^{1}H-^{1}H ROESY NMR spectrum of macrocycle **2** (2 mM) in $CDCl_3$ with TBACl (500 MHz, 298 K). The assignment started from peak g, which is unique in integration and has been confirmed in the 2D TOCSY NMR spectrum.

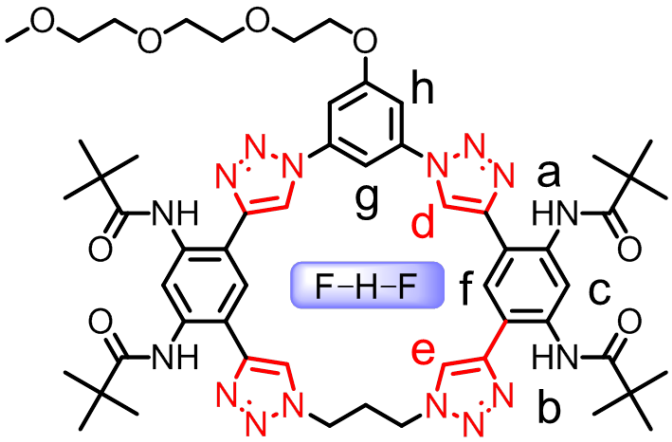

Figure S29. Summary of peak assignment for **2**•HF_2^- in $CDCl_3$.

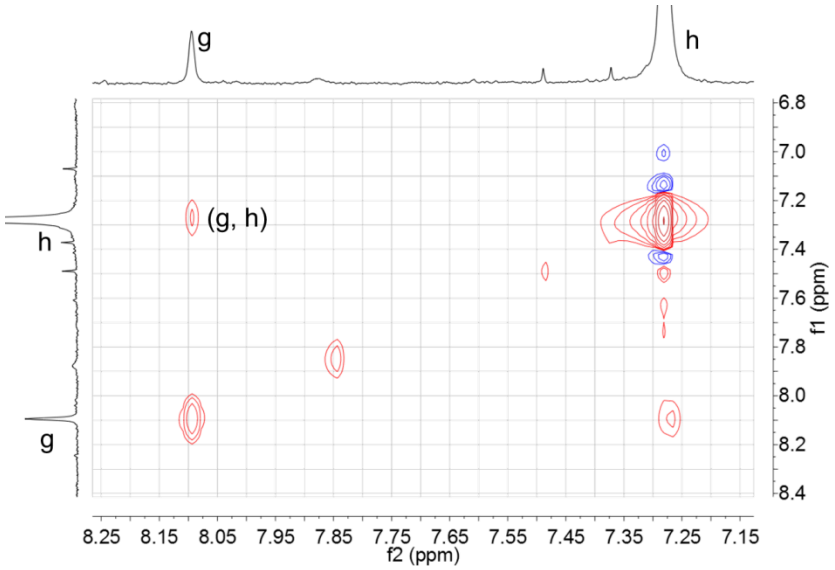

Figure S30. ^{1}H-^{1}H TOCSY NMR spectrum of macrocycle **2** (2 mM) in $CDCl_3$ with $TBAHF_2$ (500 MHz, 298 K).

S.14 UV-VIS TITRATIONS OF MACROCYCLE 2 WITH BIFLUORIDE AND CHLORIDE

UV-Vis titrations were performed and analyzed following the same procedures described in section **S.9**.

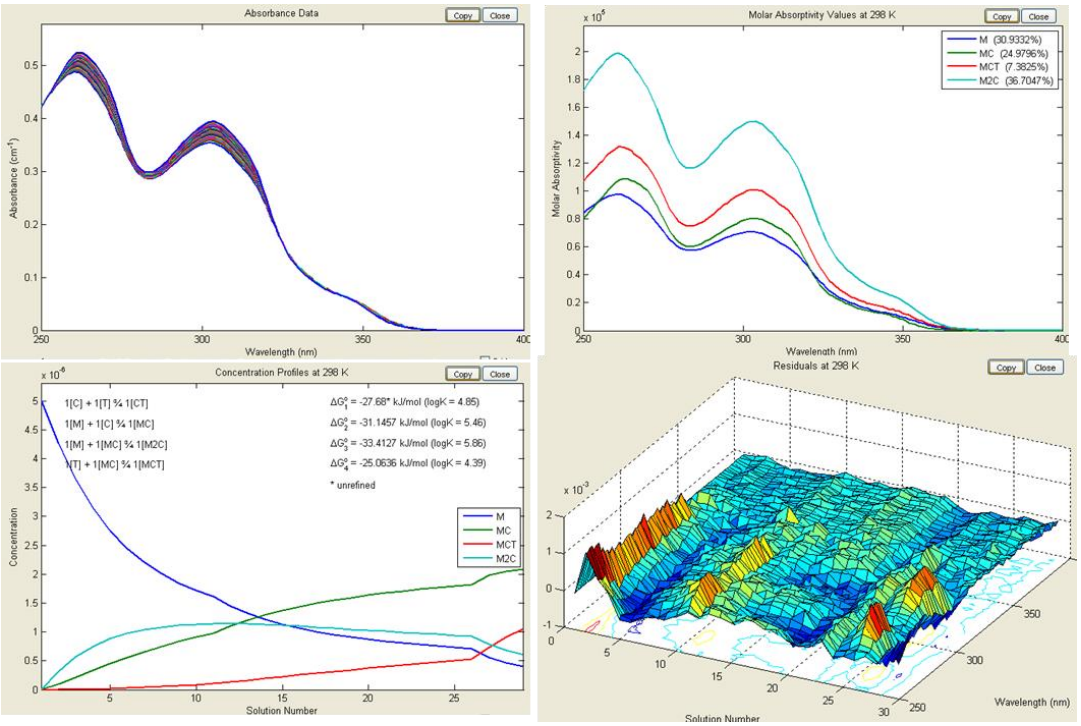

Figure S31. UV-Vis titration analysis of 1:1 complexation of **2** (5 μM) with TBACl (0–10 equivalents) in dichloromethane.

Dichloromethane Random Data Exclusion	K_1 **2** + Cl^- ⇌ **2**•Cl^-	K_{ip} TBA^+ + Cl^- ⇌ TBACl	K_2 **2**•Cl^- + **2** ⇌ $\mathbf{2}_2$•Cl^-	K_3 TBA^+ + **2**•Cl^- ⇌ TBA•**2**•Cl
None	5.46	Fixed	5.86	4.39
2 10 22 23 24	5.35		6.23	4.65
8 10 11 12 17	5.43		5.72	4.41
2 4 5 10 19	5.59		6.01	4.47
4 16 19 24 27	5.61		5.68	4.29
5 6 16 21 29	5.36		6.11	4.85
6 16 17 22 28	5.61		5.88	4.40
4 11 12 15 20	5.40		5.73	4.41
Average	5.48 ± 0.11	4.85	5.90 ± 0.20	4.48 ± 0.18

Fitting Summary: RMS Residual: 0.0002; Data Reconstruction: 99.86%; Remaining Error Imbedded in Absorbance Values: 0.01%; R^2: 99.9998%

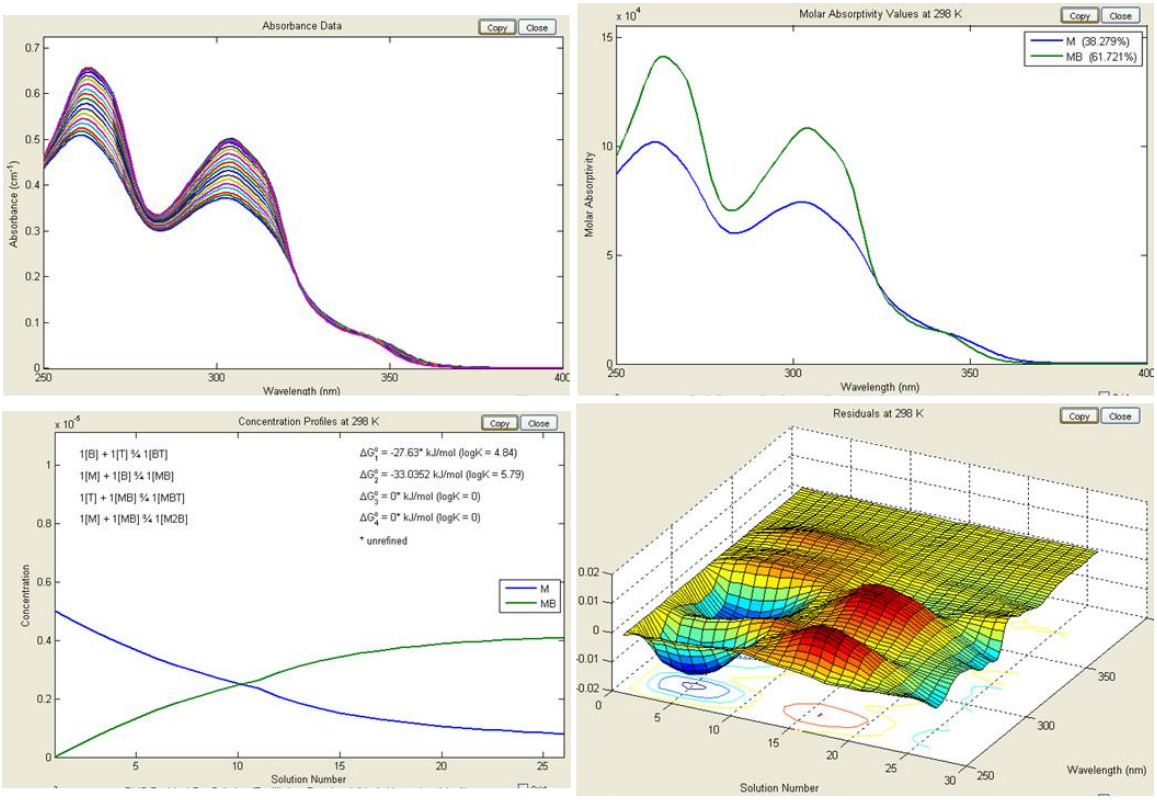

Figure S32. UV-Vis titration analysis of 1:1 complexation of **2** (5 μM) with $TBAHF_2$ (0–10 equivalents) in dichloromethane.

Dichloromethane	K_1	K_{ip}
Random Data Exclusion	**2** + HF_2^- ⇌ **2**•HF_2^-	TBA^+ + HF_2^- ⇌ $TBAHF_2$
None	5.79	Fixed
2 3 17 18 21	5.80	
7 8 12 15 22	5.83	
4 5 8 10 16	5.87	
9 14 21 25 26	5.67	
4 8 9 10 24	5.87	
9 14 15 23 25	5.71	
10 16 18 23 24	5.75	
Average	5.79 ± 0.08	4.84

Fitting Summary: RMS Residual: 0.004; Data Reconstruction: 99.20%; Remaining Error Imbedded in Absorbance Values: 0.001%; R^2: 99.97%

S.15 VARIABLE CONCENTRATION STUDIES OF MACROCYCLE 2

The aggregation of **2** in chloroform ($CHCl_3$) was investigated by variable concentration UV-Vis measurement (0.5–70 μM) at room temperature. Chloroform was used in place of dichloromethane is based on the fact that macrocycle **2** is more soluble in chloroform so that a dilution study is viable. In addition, the similar solvent properties between the two solvents may allow chloroform to be used to qualitatively evaluate the degree of self-association of **2** in dichloromethane. 4 mL of chloroform were prepared in 1 cm screw-cap quartz cell equipped with PTFE/silicone septa. Aliquots of **2** (1 mM) in chloroform prepared in screw-cap vials equipped with PTFE/silicone septa were added via 10 μL and 100 μL gas-tight micro-syringes. The absorbance at 350 nm was plotted as a function of concentration. The linear relationship between absorbance and concentration (Figure S33b) indicate that no self-association is present within the concentration range where the equilibrium constants were determined.

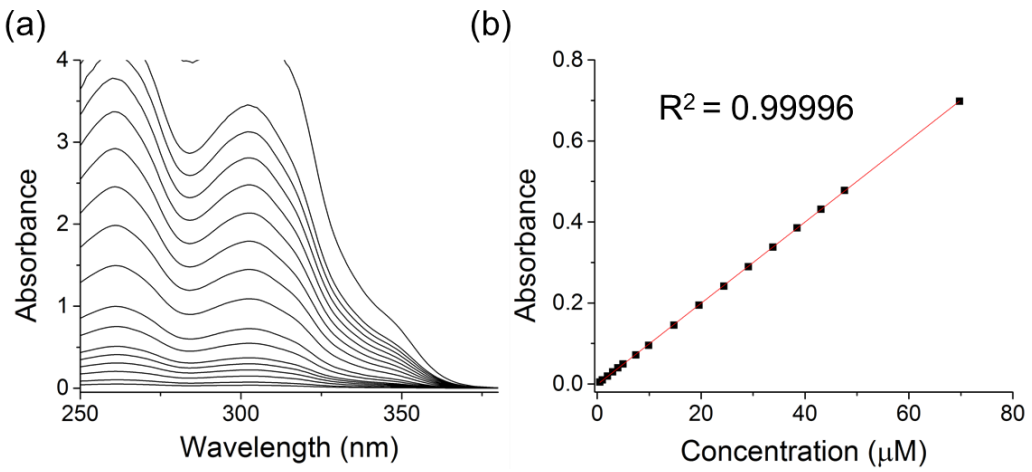

Figure S33. (a) Absorption spectra of **2** recorded in chloroform at various concentrations (0.5–70 μM). (b) The absorbance at 350 nm displayed a linear relationship with the concentration of **2**.

S.16 SPECIATION CURVES OF MACROCYCLE 2

The speciation curves were generated using the same method described in section **S.10**. In the case of chloride titration, equilibria were not simplified at lower concentrations and all of them were included in the data fitting. For bifluoride, however, similar trend was observed and thus validating the model equilibria that we have used for the UV-Vis titrations in section **S.14.**

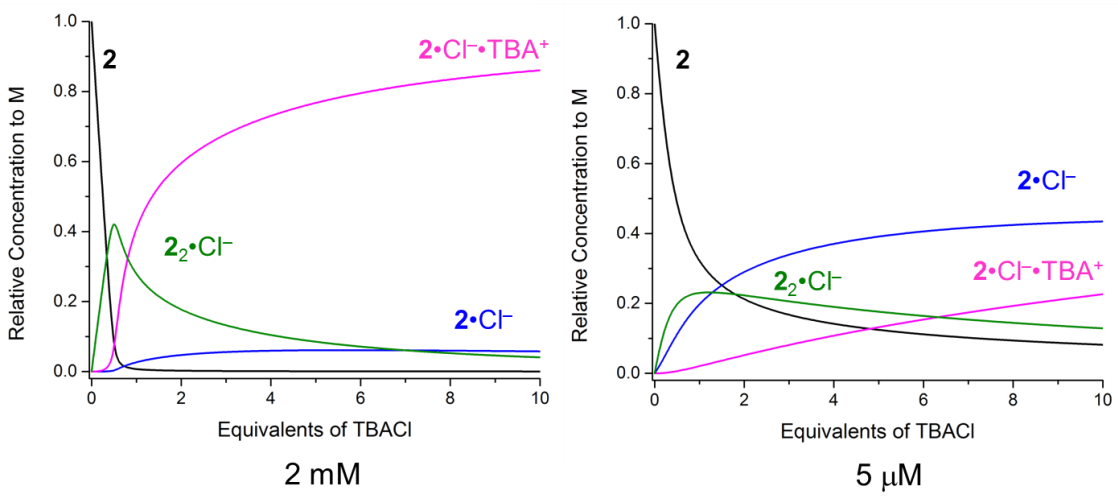

Figure S34. Speciation curve of **2** binding Cl^- in NMR titrations and UV-Vis titrations.

Table S7. Equilibrium constants associated with **2** binding Cl^- (dichloromethane, 298 K) simulated in Figure S34.

Complexes	β	Analysis Method	Method of Error Generation
2•Cl^-	5.48 ±0.11	UV-Vis (5 μM)	Sivvu
2•Cl^-•TBA^+	11.4 ±0.3	UV-Vis (5 μM)	Sivvu
TBACl	4.85 ±0.02	UV-Vis (5 μM)	Sivvu
$\mathbf{2}_2$•Cl^-	10.0 ±0.3	UV-Vis (5 μM)	Sivvu

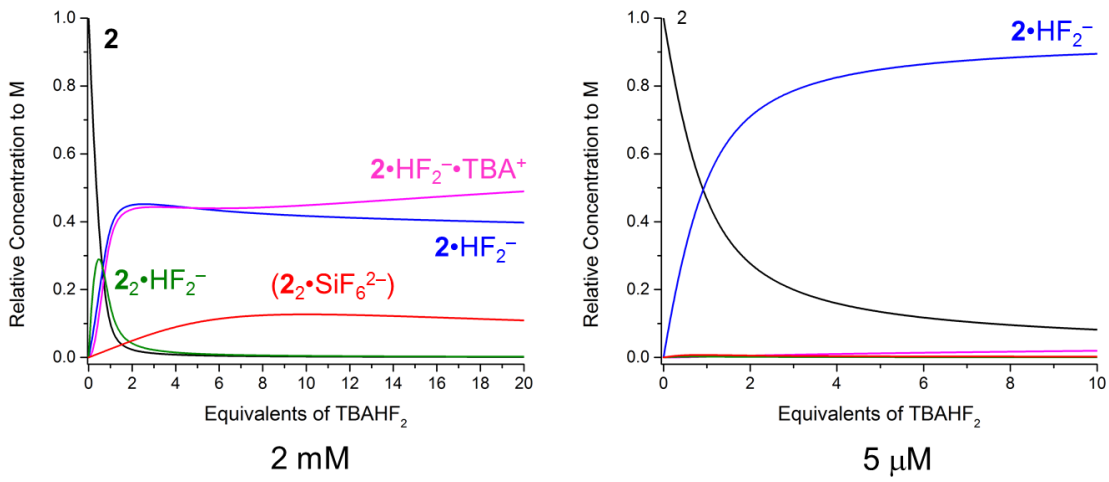

Figure S35. Speciation curve of **2** binding HF_2^- in NMR titrations and UV-Vis titrations. **2**•SiF_6^{2-} and $\mathbf{2}_2$•SiF_6^{2-} is presented as ($\mathbf{2}_2$•SiF_6^{2-}).

Table S8. Equilibrium constants associated with **2** binding HF_2^- (dichloromethane or chloroform, 298 K) simulated in Figure S35.

Complexes	β [a]	Analysis Method	Method of Error Generation
2•HF_2^-	5.79 ±0.08	UV-Vis (5 μM, CH_2Cl_2)	Sivvu
2•HF_2^-•TBA^+	8.8 ±0.1	NMR (2 mM, $CDCl_3$)	Hyss
$TBAHF_2$	4.84 ±0.02	UV-Vis (5 μM, CH_2Cl_2)	Sivvu
$\mathbf{2}_2$•HF_2^-	8.8 ±0.1	NMR (2 mM, $CDCl_3$)	Hyss
($\mathbf{2}_2$•SiF_6^{2-} + **2**•SiF_6^{2-})[b]	10.4 ±0.1	NMR (2 mM, $CDCl_3$)	Hyss

(a) The β values represent the overall formation constants. (a) Two equilibria are simulated as one apparent equilibrium leading to the formation of 2:1 ion-pair complex $\mathbf{2}_2$•SiF_6^{2-}. β = /[$\mathbf{2}_2$•SiF_6^{2-}] / ([**2**]^2[SiF_6^{2-}]).

S.17 NMR SPECTRA OF SYNTHESIZED COMPOUNDS

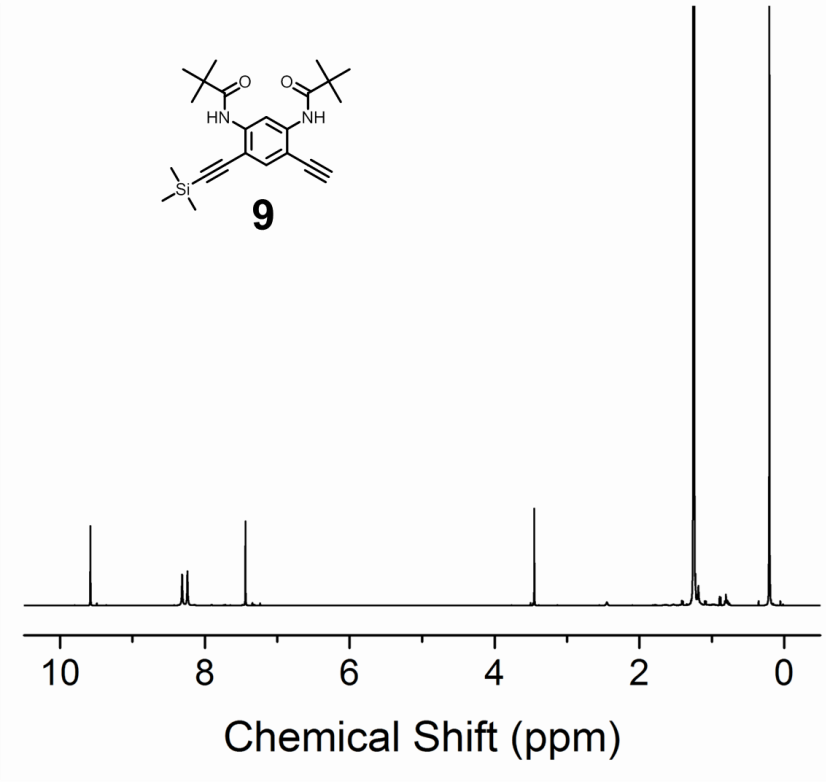

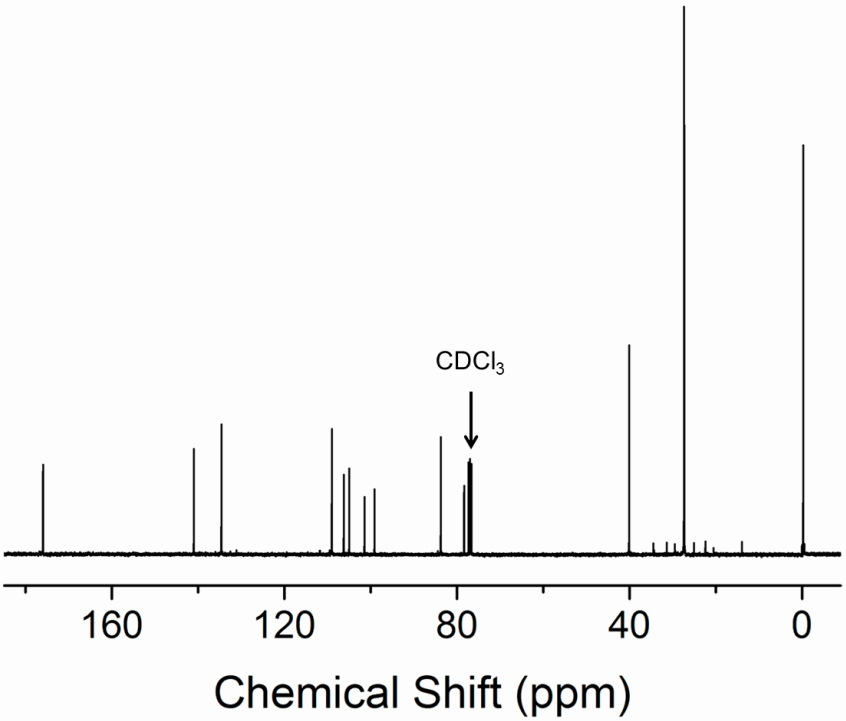

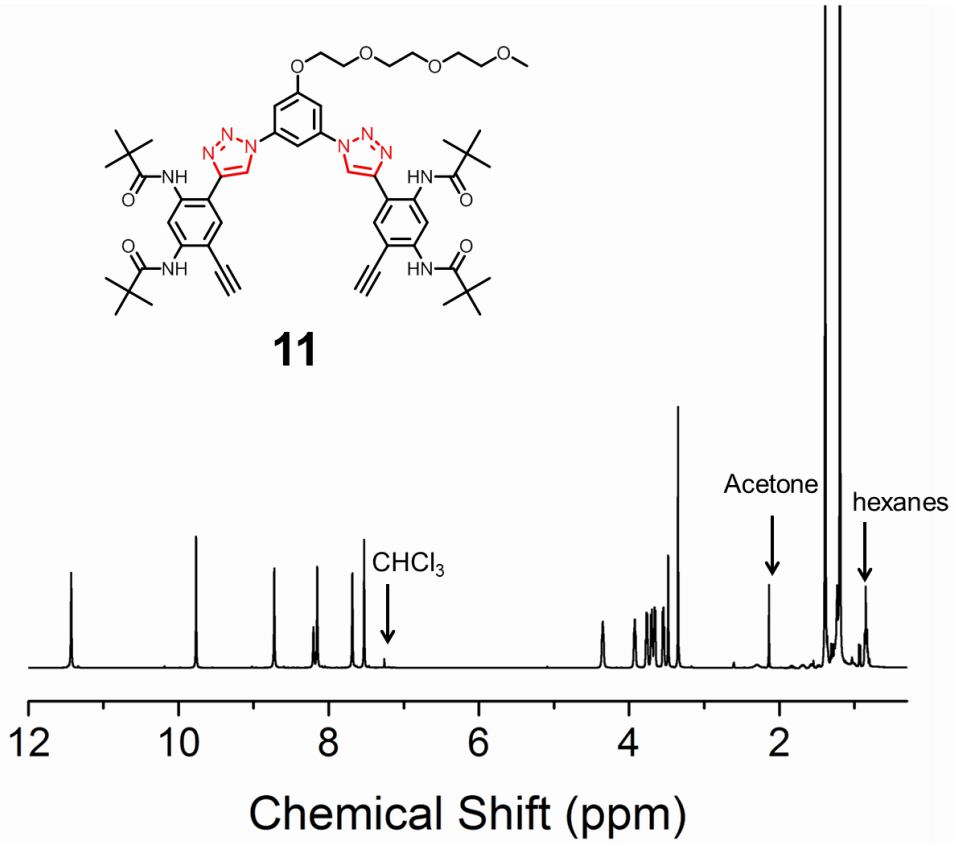
11
Acetone
hexanes
CHCl3
12
10
8
6
4
2
Chemical Shift (ppm)

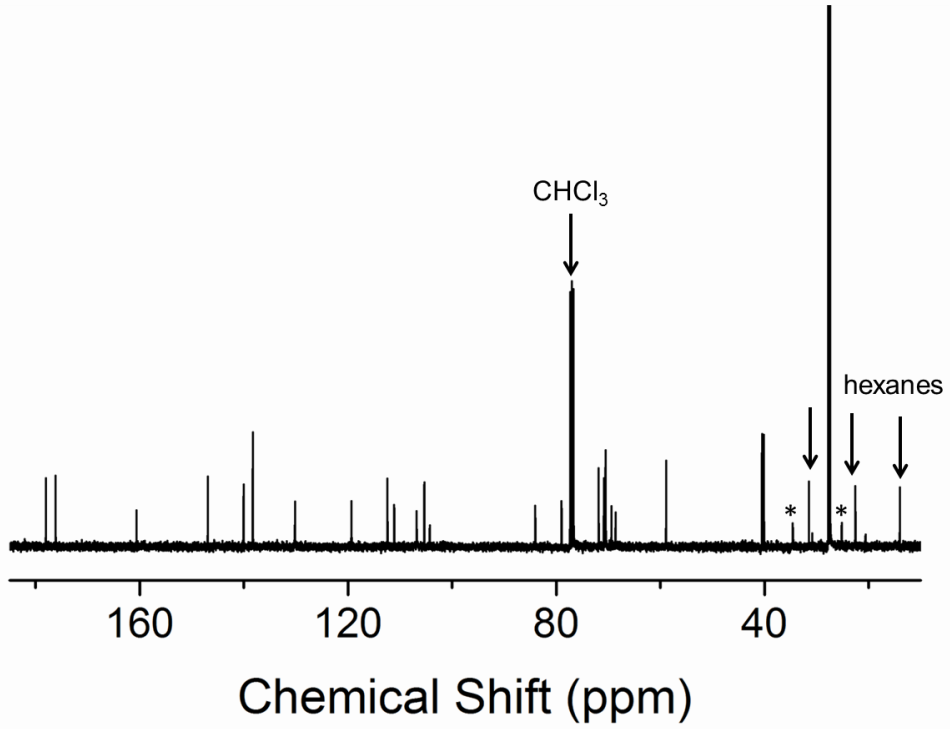
CHCl3
hexanes
*
*
160
120
80
40
Chemical Shift (ppm)

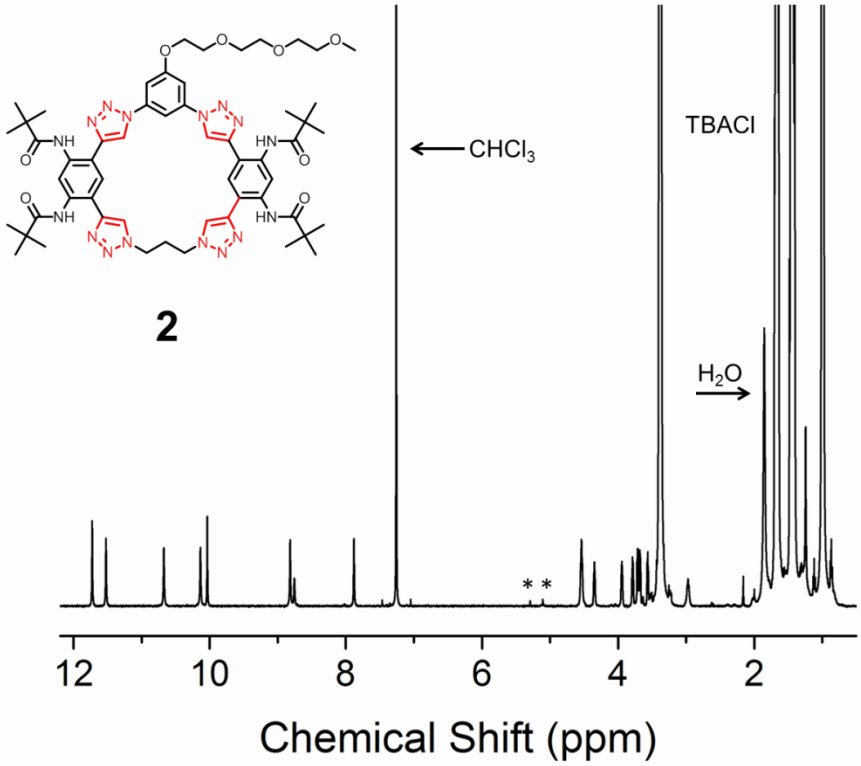
2
CHCl3
TBACl
H2O
12
10
8
6
4
2
Chemical Shift (ppm)

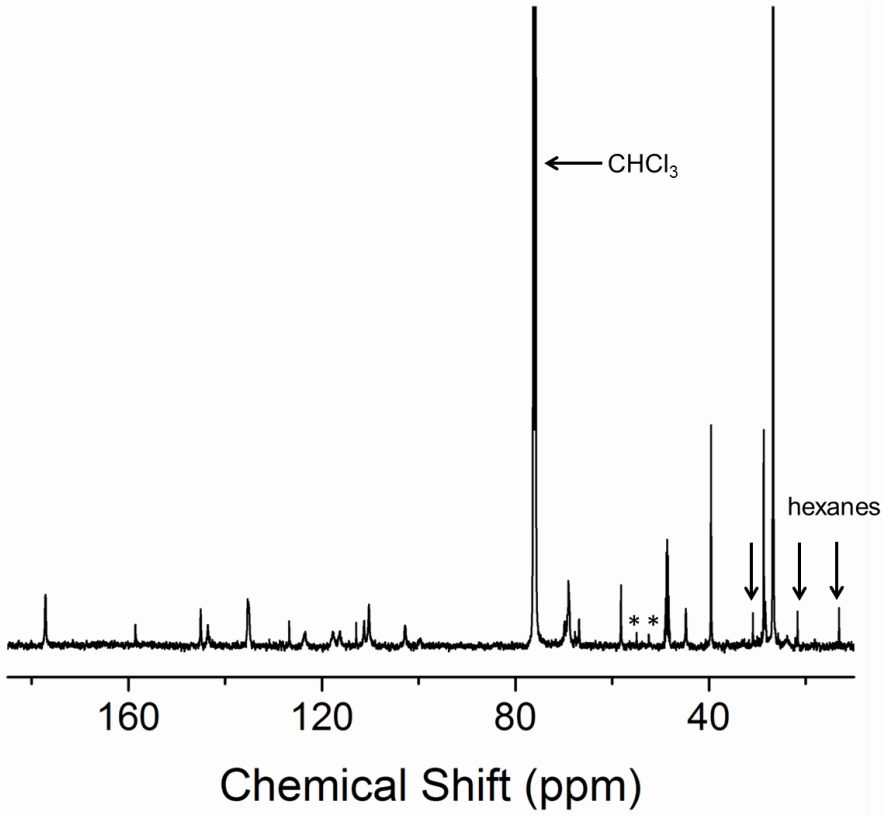
CHCl3
hexanes
160
120
80
40
Chemical Shift (ppm)

S. 18 DISPERSION EFFECTS AND RELATIVE SOLVATION ENERGIES

Table S9. The inclusion of dispersion effects[a] upon the binding energies on all the minima are noted to not have any significant impact

Macrocycle	Anion	Dispersion correction to binding energies in kcal / mol
3	Chloride	− 0.43
3	Bifluoride[b]	− 0.71
3	Bifluoride[c]	− 0.71
4	Chloride	− 0.47
4	Bifluoride	− 0.74

(a) Grimme's dispersion correction to the M06-2X functional with the zero-damping function was used. (b) Corresponds to NS mode. (c) Corresponds to EW mode

Table S10. Single-point solvation calculations are consistent with the experimentally obtained relative free-energies[a] between: (i) the different modes of bifluoride binding with the parent triazolophane and (ii) chloride and bifluoride binding with the amide-based macrocycle

Macrocycle	Anion	Computed Free-energy[b] in DCM (kcal / mol)	Computed Free-energy[c] in DCM (kcal / mol)
3	Bifluoride[d]	− 2.43	− 1.65
3	Bifluoride[e]	−1.33	− 0.63
4	Chloride	− 3.14	− 2.67
4	Bifluoride	− 2.11	− 1.37

(a) Solvation models however, do not accurately reproduce the experimentally obtained absolute free-energies in solution. (b) Grimme's dispersion correction to the M06-2X functional with the zero-damping function was used. (c) Without including dispersion corrections. (d) Corresponds to NS mode. (e) Corresponds to EW mode.

References

1 Li, Y.; Flood, A. H., *J. Am. Chem. Soc.* **2008**, *130*, 12111–12122.

2 McDonald, K. P.; Ramabhadran, R. O.; Lee, S.; Raghavachari, K., Flood, A. H., *Org. Lett.* **2011**, *13*, 6260–6263.

3 LoCoco, M. D.; Zhang, X.; Jordan, R. F., *J. Am. Chem. Soc.* **2004**, *126*, 15231–15244.

4 (a) Vander Griend, D. A.; Bediako, D. K.; DeVries, M. J.; DeJong, N. A.; Heeringa, L. P. *Inorg. Chem.* **2008**, *47*, 656–662. (b) Li, Y.; Vander Griend, D. A.; Flood, A. H. *Supramol. Chem.* **2009**, *21*, 111–117.

5 Frisch, M. J. *et al.* Gaussian Development Version, Revision H.08; Gaussian Inc.: Wallingford, CT, **2010**.

6 Zhao, Y.; Truhlar, D. G. *Theor. Chem. Acc.* **2008**, *120*, 215–241.

7 Mayer, I.; Surjan, P. R. *Chem. Phys. Lett.* **1992**, *191*, 497–499.

8 (a) Christe, K. O.; Wilson, W. W. *J. Fluorine Chem.* **1990**, *46*, 339–342. (b) Gelmboldt, V. O.; Ganin, E. V.; Fonari, M. S.; Simonov, Y. A.; Koroeva, L. V.; Ennan, A. A.; Basok, S. S.; Shova, S.; Kahlig, H.; Arionf, V. B.; Kepplerf, B. K. *Dalton Trans.* **2007**, 2915–2924.

9 (a) Morgan, G.; McKee, V.; Nelson, J. *J. Chem. Soc., Chem. Commun.* **1995**, *16*, 1649–1652. (b) Mason, S.; Llinares, J. M.; Morton, M.; Clifford, T.; Bowman-James, K. *J. Am. Chem. Soc.* **2000**, *122*, 1814–1815.

10 Marat, R. K.; Janzen, A. F. *Can. J. Chem.* **1977**, *55*, 3845–3849.

11 S. Alunni, A. Pero, G. J. Reichenbach, *Chem. Soc., Perkin Trans. 2* **1998**, 1747–1750.

12 Hua, Y.; Ramabhadran, R. O.; Uduehi, E. O.; Karty, J. A.; Raghavachari, K.; Flood, A. H. *Chem. Eur. J.* **2011**, *17*, 312–321.

13 Ramabhadran, R. O.; Hua, Y.; Li, Y.-J.; Flood, A. H.; Raghavachari, K. *Chem. Eur. J.* **2011**, *17*, 9123–9129.

14 Kang, S. O.; Powell, D.; Day, V. W.; Bowman-James, K. *Angew. Chem. Int. Ed.* **2006**, *45*, 1921–1925.

15 L. Alderighi, P. Gans, A. Lenco, D. peters, A. Sabatini, A. Vacca, *Coord. Chem. Rev.* **1999**, *184*, 311–318.